Astronomy & Astrophysics manuscript no. niki1˙v3
November 18, 2011

Spectra probing the number ratio of C- to M-type AGB stars in the NGC 6822 galaxy ⋆, ⋆⋆

N. Kacharov[1,2,3], M. Rejkuba[1], and M.-R. L. Cioni[4,5]⋆⋆⋆

[1] ESO, Karl-Schwarzschild-Strasse 2, D-85748 Garching, Germany
[2] Institute of Astronomy, Bulgarian Academy of Sciences, 72 Tsarigradsko Chaussee Blvd., 1784 Sofia, Bulgaria
[3] Department of Astronomy, St. Kliment Ohridski University of Sofia, 5 James Bourchier Blvd., 1164 Sofia, Bulgaria
[4] University Observatory Munich, Scheinerstrasse 1, 81679 München, Germany
[5] University of Hertfordshire, Physics Astronomy and Mathematics, Hatfield AL10 9AB, United Kingdom

Received: 31.05.2011 / Accepted: 16.10.2011

ABSTRACT

Aims. We calibrate spectroscopically the C- versus (vs.) M-type asymptotic giant branch (AGB) star selection made using near-IR photometry, and investigate the spatial distribution of the C/M ratio in NGC 6822, based on low resolution spectroscopy and near-IR photometry.

Methods. We obtained low resolution multi-object spectroscopy with the VIMOS instrument at the ESO VLT of ∼ 800 stars in seven fields centred on NGC 6822. The spectroscopic classification of giant stars in NGC 6822 and foreground dwarf contaminants was made by comparing more than 500 good quality spectra with the spectroscopic atlas of Turnshek et al. (1985). The sample of spectroscopically confirmed AGB stars in NGC 6822 is divided into C- and M-rich giants to constrain the C vs. M AGB star selection criteria based on photometry. The larger near-IR photometric sample is then used to investigate the C/M ratio gradients across the galaxy.

Results. We present the largest catalogue of near-IR photometry and spectra of AGB stars in NGC 6822 with 150 C-stars and 122 M-stars. Seventy-nine percent of the C-stars in our catalogue are redder than $(J-K)_0 = 1.2$ mag, and 12% are brighter than $K_0 = 16.45$ mag and bluer than $(J-K)_0 = 1.2$ mag. The remaining 9% are mixed with the M-type AGB stars, 88% of which have colours $(J-H)_0 > 0.73$ mag and $(J-K)_0$ between 0.9 mag and 1.2 mag. The remainder are mixed with dwarfs and C-type stars. The foreground dwarfs have preferably colours $(J-H)_0 < 0.73$ mag (95%). Using the proposed criteria, we estimate that the overall C/M ratio of the galaxy is around 0.8 with a spread between $0.2 < \mathrm{C/M} < 1.8$. These results suggest that the metallicity index [Fe/H] is between −1.2 dex and −1.3 dex according to the different calibrations and that there is a significant spread of about $0.4 \div 0.6$ dex. We also discuss age rather than metallicity variations that could explain the C/M ratio trends.

Key words. Galaxies: irregular, dwarf galaxies, local group – Galaxies: Individual: NGC 6822 – Galaxies: stellar content – Stars: AGB stars, C- and M-type stars

1. Introduction

The intermediate-age asymptotic giant branch (AGB) stars are classified as carbon-rich (C stars) or oxygen-rich (M stars), depending on which element dominates their atmosphere. These stars are among the most luminous stars in a galaxy in near-IR, and are thus easily observable at large distances. The upcoming large telescopes (> 20 m) will operate most efficiently in near-IR and will detect large samples of AGB stars in nearby galaxies. In Addition, this stellar evolutionary phase is extremely important to the studies of high redshift galaxies, because these relatively young galaxies contain significant fraction of intermediate-age stars, and in a 1 Gyr old simple stellar population up to 80% of the K-band light originates from the luminous AGB stars (Maraston 2005; Maraston et al. 2006). Nevertheless, the intermediate-age stellar evolutionary models, the stellar atmospheres, the internal composition, and the physics of luminous AGB stars are all affected by large uncertainties (Cassisi et al. 2001; Gallart et al. 2005; Ventura & Marigo 2010), and currently this is one area of stellar evolutionary theory where important improvements are needed, both theoretically (Marigo & Girardi 2007; Marigo et al. 2008) and observationally (e.g. Girardi & Marigo 2007; Lyubenova et al. 2010; Girardi et al. 2010).

At present, the selection of C and M stars is made using either near-IR colour-magnitude diagrams or colour-colour diagrams for broad- and narrow-band filters (Battinelli & Demers 2004). These surveys rely on photometric selection criteria that have inherent uncertainties, do not easily distinguish K giants and Galactic M dwarfs, and do not account for S-type stars. The situation somewhat improves, at least for K giants, if optical and IR selection criteria are used together (Cioni & Habing 2005). The spectroscopic classification of AGB stars covering a range of metallicities is necessary to properly estimate the biases and establish quantitative criteria for the photometric selection boxes.

The C/M ratio is the number ratio of C-type (carbon-rich) to M-type (oxygen-rich) AGB stars. It is a function of the [Fe/H] abundance (Battinelli & Demers 2005) and provides a

Send offprint requests to: N. Kacharov, kacni@abv.bg

⋆ Based on observations made with ESO telescopes at the La Silla Paranal Observatory under programme ID 383.D-0367

⋆⋆ Complete Table 2 and the reduced spectra in ASCII format are available at the CDS via anonymous ftp to cdsarc.u-strasbg.fr (130.79.128.5).

⋆⋆⋆ Research Fellow of the Alexander von Humboldt Foundation

simple indication of the metallicity distribution across galaxies (e.g. Cioni et al. 2008, 2009; Cioni & Habing 2003, for M 33 and the Magellanic Clouds, respectively). The C/M vs. [Fe/H] relation is due to the combined effect of pronounced carbon dredge-up on the stellar spectrum at low metallicity, and the blue colours of metal-poor red giants (Iben & Renzini 1983). The lower metallicity O-rich stars turn into C-type AGB stars more easily and remain so for a longer time than those of higher metallicity because fewer carbon atoms need to be dredged up to effect this transformation, and in addition at lower metallicity the AGB evolutionary tracks have higher temperatures, which causes lower abundances of TiO molecules, hence smaller numbers of M stars. However, while theoretically clear arguments exist for the dependence of C/M ratio on [Fe/H], the relation is still poorly calibrated owing to: (i) the ill-defined criteria for selecting C and M stars; (ii) the contamination from both foreground and S stars (S stars have equal amounts of carbon and oxygen in their atmospheres); and (iii) the need to have a well-defined sample of AGB stars with spectroscopically determined metallicites.

The NGC 6822 galaxy is an ideal target for the study of C- and M-type AGB stars and the C/M ratio as a function of metallicity. It is a relatively well-studied dwarf irregular galaxy in the constellation Sagittarius at a distance of $\sim$ 490 kpc (Mateo 1998). Owing to its low Galactic latitude ($b = -18.39°$), it is affected by moderate foreground extinction, $E(B-V) = 0.24$ mag (Schlegel et al. 1998). It is similar in mass ($1.9 \times 10^9\ M_\odot$), structure, and metallicity ($\sim 0.2\ Z_\odot$) to the Small Magellanic Cloud and consists of different morphological components (disk, bar, and halo), rotation, gas content, active star formation, and dark matter distribution (Weldrake et al. 2003). Star formation in this galaxy began at least 10 Gyr ago (Clementini et al. 2003) and remains ongoing (Gallart et al. 1996; Hutchings et al. 1999). The galaxy is embedded in a large HI envelope (Weldrake et al. 2003). Previous spectroscopic studies, although incomplete, of supergiants (Venn et al. 2001), HII regions (Chandar et al. 2000), and red giant branch (RGB) stars (Tolstoy et al. 2001) found evidence of a gradient in [O/H] and measured an average [Fe/H] = −0.9 dex with a spread of 1.5 dex. Most importantly, this galaxy has a large and widely distributed intermediate-age population (Battinelli et al. 2006) with a clear spread in metallicity (Cioni & Habing 2005). The C/M ratio has been estimated photometrically both from optical and near-IR criteria. This work provides the first comprehensive *spectroscopic* study of the AGB population of NGC 6822 dwarf irregular galaxy and its metallicity distribution.

We initiated a project to improve the C/M vs. [Fe/H] calibration using the large sample of intermediate-age stars in NGC 6822, for which we have a large database of near-IR photometry, low-resolution optical spectra useful to spectroscopically select C- and M-type AGB stars, as well as near-IR Ca II triplet spectroscopic observations used to indirectly measure [Fe/H]. Our preliminary results for the near-IR photometry were presented by Sibbons et al. (2010), and their full analysis is in preparation. This work analyses the near-IR optical spectra obtained with VIMOS multi-object spectrograph at the ESO VLT, and in a future article we will present the near-IR Ca II spectroscopic observations of AGB stars in NGC 6822.

2. Observations and data reduction

Our spectroscopic survey of M- and C-type AGB stars in the dwarf irregular galaxy NGC 6822 was made using the VIMOS imager and multi-object spectrograph (Le Fèvre et al. 2003) at the ESO VLT UT3 telescope. The instrument is mounted on the Nasmyth B focus of UT3 Melipal and has four identical arms, each with a $\sim 7' \times 8'$ FOV and a $0\farcs205$ pixel size. The gap between the quadrants is $\sim 2'$ and each quadrant is equipped with one EEV $2\text{k} \times 4\text{k}$ CCD.

We first obtained mandatory R-band pre-imaging observations of seven fields in NGC 6822 in service mode. These pre-images were then used together with the wide field near-IR photometric catalogue obtained at UKIRT with WFCAM (Sibbons et al. 2010, Sibbons et al. 2011, in prep), to prepare the multi-object masks for spectroscopic follow-up observations in visitor mode, which comprised four masks (one per VIMOS quadrant) for each pointing.

We targeted seven fields, four centred on NGC 6822, and two outer fields. The central field had two different mask sets, each with 100-120 targets, while the other six fields had each one set of masks. In total, we targeted $\sim$ 800 stars in eight setups. The spectroscopic target selection was based on the UKIRT near-IR photometric data. All discussed magnitudes and colours in this study were corrected for foreground extinction according to the Schlegel et al. (1998) extinction map. All selected targets are brighter than 17.45 mag in K_0 and have $(J-K)_0 > 0.74$ mag, although redder stars were targeted preferentially. Cioni & Habing (2005) detected the RGB tip (TRGB) at $K_s = 17.10 \pm 0.01$ mag, while Sibbons et al. (2010) report that it varies across the galaxy by $\Delta K = 1.36$ mag, with an average value of $K = 17.48 \pm 0.26$ mag. Davidge (2003) adopted a distance modulus of 23.49 mag based on the Cepheid and RGB tip measurements of Gallart et al. (1996), and measured the onset of the RGB tip in K band near $K = 17$ mag. This is consistent with $M_K^{\rm RGBT} \sim -6.5$ mag. Gorski et al. (2011) identified the TRGB at $K = 16.97 \pm 0.09$ mag.

Our observing log is presented in Table 1. In the second last column (slits), we report the number of slits for each pointing (sum of slits in four VIMOS quadrants), and in the last column (stars) we list the number of good quality recorded spectra (quality flags: 4, 5, or 6; see below) for each observed setup.

For our spectroscopic observations on August 22-24, 2009, we used the medium resolution grism (MR grism) and GG475 order sorting filter, which provides a spectral resolution $R = 580$ (2.5 Å/pix dispersion) and a wavelength coverage from 500 to 1000 nm. The severe fringing in the red for the old VIMOS thinned and back-side illuminated, single-layer coated CCDs, used until May 2010 (Hammersley et al. 2010), meant that there was a significantly more restricted useful wavelength range of 500-780 nm in our spectra. Each setup was exposed for 2×20 min.

We used the ESO VIMOS pipeline (version 2.5.2) to reduce the spectra. For each of the two observing nights, we took separate sets of bias frames and spectrophotometric standard-star observations. The reduction and extraction of the scientific exposures was performed in three steps with the following pipeline recipes. First we used the *vmbias* recipe to create a master bias frame averaging the five bias frames. The *vmmoscalib* recipe was then used to obtain the wavelength calibration from the arc lamp spectra, trace the edges of the associated flat fields, and prepare all necessary tables for the scientific extraction.

We note that the flat-field exposures were only used to trace the slit edges and prepare the extraction tables. We decided not to apply a flat-field correction to our target spectra, as the flat fields were taken in the morning after the observing night. The different rotator angle and small differences in the positioning of the masks in the focal plane of the instrument may cause small shifts between the flat-field and science exposures, which could

Table 1. Observing log.

Night	Field	RA [hh:mm:ss]	DEC [° : ′ : ″]	Exposure [s]	Slits	Stars
22-23 Aug. 2009	CF1	19:44:56.75	−14:48:14.18	2 × 1200	119	57
	CF2	19:44:56.75	−14:48:14.18	2 × 1200	108	81
	NW1	19:44:20.77	−14:40:53.26	2 × 1200	108	47
	NE1	19:45:31.78	−14:40:52.64	2 × 1200	114	96
	SE1	19:45:33.78	−14:55:45.77	2 × 1200	123	115
23-24 Aug. 2009	SW1	19:44:19.78	−14:55:43.03	2 × 1200	101	62
	NE2	19:48:17.18	−14:24:45.94	2 × 1200	78	70
	SW2	19:42:09.78	−15:14:40.20	2 × 1200	70	18

then cause a decrease in the signal-to-noise ratio (S/N) after flat-fielding. We experimented with applying the flat-field correction but found that this neither improved nor decreased the spectrum S/N in the blue, while in the red part owing to fringing, spectra that were flat-fielded were actually noisier. We only find a difference in the third quadrant, where all exposures display some artificial drop in efficiency for certain wavelength ranges (most significantly around the sodium doublet, as most clearly seen in Fig. 5), which could not be fully corrected by applying a flat-field correction. This, however, did not affect our spectral classification.

The *vmmosscience* recipe was used to extract and calibrate the target spectra. This recipe applies the extraction mask obtained with *vmmoscalib*. The slit spectra are bias subtracted and remapped by eliminating the optical distortions. An additional wavelength calibration adjustment was made by fitting several strong sky emission lines. The final mean model accuracy of the wavelength calibration is about 0.15 pix, but the measurements of sky line offsets with respect to the expected wavelength sometimes have values of up to several pixels for individual spectra (Fig. 1).

We had acquired two scientific exposures for each observed field, which were aligned and stacked together. We adopted local sky subtraction and cosmic cleaning, and the optimal extraction method (Horne 1986) within the *vmmosscience* recipe. Finally, we applied the response curve, obtained from a spectrophotometric standard star observation. The reduction process of the standard star observations was analogous to the scientific ones. During the entire reduction process, we manually checked all spectra to verify spectral tracing, wavelength calibration, and object detection.

Unfortunately, the low resolution of our spectra and the very broad spectral features, prevented accurate measurements of the radial velocities of the targeted stars. On the basis of the Besançon model of our Galaxy (Robin et al. 2003), the expected median radial velocity and its standard deviation for the Milky Way foreground population of stars with $15 < K < 17.5$ mag in the direction of NGC 6822 is 1 ± 44 km/s. Owing to the overlap of this distribution with the radial velocity of NGC 6822 (−57 km/s), which is based on HI data (Koribalski et al. 2004), and the radial velocities of the carbon stars obtained by Demers et al. (2006b) (between +10 and −70 km/s ±15 km/s), combined with the uncertainty in our measured radial velocities, we decided not to rely on radial velocities to distinguish between the foreground dwarfs and NGC 6822 giant star members, but to instead use spectral features to distinguish the two populations. The classification of spectral types for all acquired spectra is described in Sect. 3.

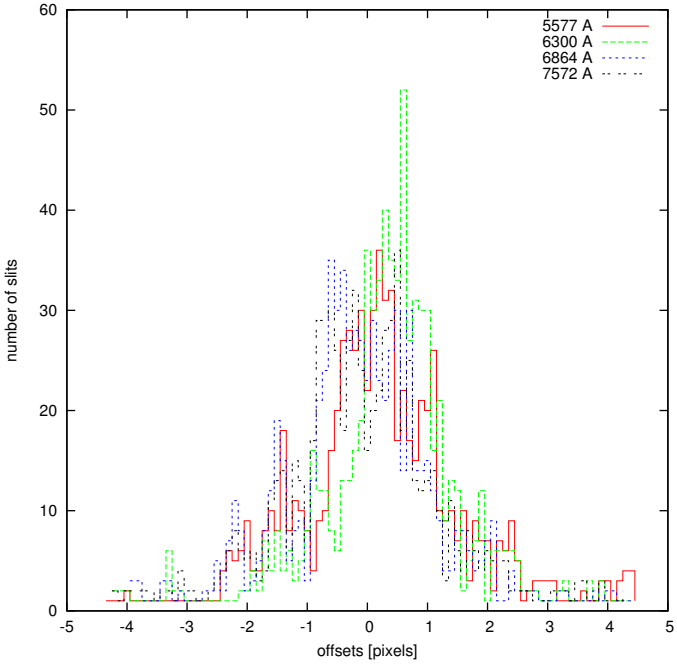

Fig. 1. Distribution of offsets in pixels for four sky lines with respect to their expected wavelengths.

We used SExtractor (Bertin & Arnouts 1996) to derive R-band photometry from the pre-imaging, which was then calibrated using the NOMAD catalogue (Zacharias et al. 2005) based on about 200 stars in common with our observations. The calibration is presented in Fig. 2. We tested two fits to the data, a linear and a constant shift, which are presented in Eq. 1 and 2.

$$R_{\rm NOMAD} = 1.08^{\pm 0.02} \times R_{\rm pre-imaging} + 2.87^{\pm 0.27} \quad (RMS = 0.24), \quad (1)$$

$$R_{\rm NOMAD} = R_{\rm pre-imaging} + 4.03^{\pm 0.02} \quad (RMS = 0.25). \quad (2)$$

In obtaining the R-band photometry, we used the linear fit calibration (Eq. 1). All R-magnitudes were corrected for interstellar extinction according to Schlegel et al. (1998) using the NED extinction-law calculator. We note that the errors in the R-band photometry are larger than the errors of the IR-photometry because the NOMAD catalogue is a compilation of data from different sources.

3. Spectral classification

For each of our spectroscopic targets, we compiled near-IR photometric data based on the UKIRT photometry (Sibbons et al.

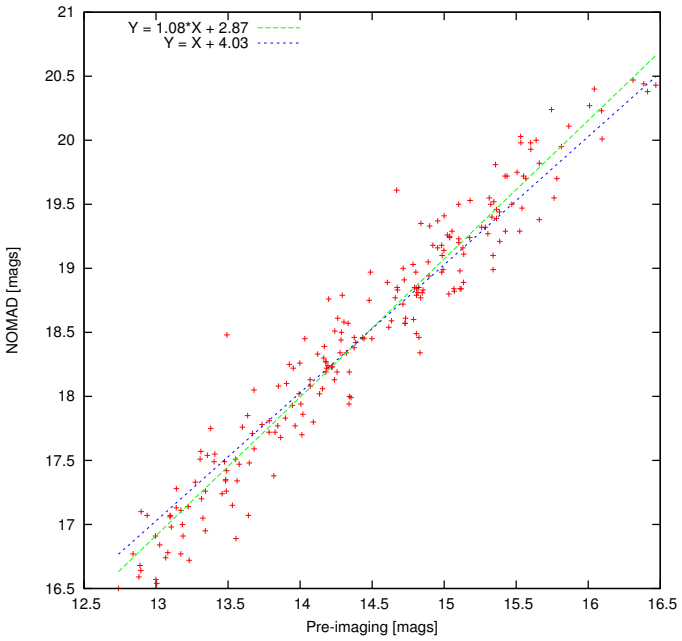

Fig. 2. R-band pre-imaging calibration. The lines are fits to the data indicated by the equations given within the figure.

2010) and complemented this with the spectral type based on reduced VIMOS spectra.

We determined the spectral class of each star mainly by visual comparing our spectra with those in the "Atlas of digital spectra of cool stars" (Turnshek et al. 1985). Where possible, we also compared our spectra with the spectral library of Jacoby et al. (1984). This spectral library is unfortunately less complete, in particular, there are not C-rich giants. To match the resolution of our spectra to that of the spectral atlas, and reduce the noise, we smoothed our spectra with a level 5 boxcar smoothing function using the *splot* IRAF task. Each spectrum was assigned one of the following quality flags, which are based primarily on the clarity of the spectral features, and not on the S/N: flag 2 for no detection; flag 3 for a poor quality spectrum, the star cannot be classified; flag 4, when we can determine whether the star is M- or C-type and eventually whether it is a giant or a foreground dwarf; flag 5 for very good quality spectra, the error in the spectral classification is within ± one subtype; and flag 6 for an excellent quality and precise determination of the spectral class. The stars with lowest quality flags (2 or 3) were excluded from our final list. Fig. 3 shows typical examples of spectra with different quality flags. We indicate in this figure on top the primary spectral features that were used to assign a spectral type to M giants.

Typical M giants are characterized by TiO absorption bands, which are stronger for increasingly later spectral types. The telluric features O_2 and H_2O are present in all spectra, because we did not apply a telluric correction, and are indicated at the bottom of the figure. The C-type giants can be quite easily distinguished as they have characteristic C_2 and CN molecular bands. The S-type stars display ZrO absorption features.

After we had performed an initial "by eye" spectral classification, we rescaled all spectra to an equal flux level and plotted them separately for each spectral sub-class to verify that indeed all spectra that had been assigned to that spectral sub-class had similar spectra. If an outlier was found, its spectral classification was repeated by comparing its spectrum with average spectra for different adjacent spectral classes. For each spectral subtype, we compiled an average spectrum. Fig. 4 compares spectra of all M4 giants (green lines) with the spectrum from Jacoby et al. (1984) (dotted blue line), as well as the average M4 giant spectrum (red thick line). Similarly, Fig. 5 compares M0 dwarf spectra (green) with the average spectrum (red) and the M0 dwarf spectrum from Jacoby et al. (1984) (dotted blue line). We note that the molecular bands of the reference spectra from Jacoby et al. (1984) library are deeper, than those of average NGC 6822 spectra, most probably because of the higher metallicity of Milky Way stars. We tried to find information about the metallicities of the used reference stars in the Pastel database (Soubiran et al. 2010) but found data for only two reference giants, which both have solar metallicity. A comparison of synthetic spectra of different metallicities from the standard stellar library of Lejeune et al. (1997) reveals some differences in the depths of the main molecular bands and the shapes of the spectra. The stars of higher metallicity appear to have slightly later subtype than those of lower metallicity, at a given temperature and gravity. This means that our spectral classification of the M-type giants might be slightly underestimated, because of the lower average metallicity of NGC 6822 with respect to stars in the comparison spectral atlases (Turnshek et al. 1985; Jacoby et al. 1984), which are principally located in the solar neighbourhood.

The wide absorption feature around the Na I line in some of the M dwarf spectra (shown with green lines) in Fig. 5 is caused by flat field residuals. All spectra displaying these artifacts were acquired on the third quadrant CCD. We note that they are not real features. We note that all bands in the Jacoby et al. (1984) M0 V spectrum appear deeper than in our M0 V spectra. This is due to differences between the reference libraries. The M0 V spectral class of Jacoby et al. (1984) is indeed more consistent with the M1 V spectral class of Turnshek et al. (1985), which is our primary reference. Unfortunately, we could not find information about the metallicities of these reference stars in the literature.

Table 2 shows part of our final spectroscopic catalogue, the full version of which is available in electronic format. Column ID is the identifier of the stars, X and Y are the positions of the stars in the VIMOS pre-images, and column r is the distance from the centre of NGC 6822 (RA = 296.24059, DEC = −14.80343). The other columns list the R_0, J_0, H_0, and K_0 magnitudes, the photometrically assigned spectral class (Sibbons et al. 2010), the classification based on our VIMOS spectra, and in the last column the quality flag of the spectra.

Different spectral subtypes are presented according to our classification in Fig. 6. The most similar dwarf and giant average spectra are plotted one over the other for comparison. It is easy to follow the change of some of the spectral features characteristic of M-type stars with increasing subtype. The strong sodium doublet (blended into a single line at our resolution) is the most typical feature of luminosity class V stars. With increasing subtype, it becomes weaker and dominated by the TiO band in the same wavelength range. For the later class dwarfs, we used the CaH molecular band at 6946Å, which deepens and widens the TiO bands in this region, to distinguish foreground dwarfs from giants. Another typical feature of the dwarf stars is the MgH band at 5211Å. The very late-type M dwarfs often display Hα in emission, which may be evidence of magnetic activity. However, Hα was not used as a criterion for distinguishing dwarfs from giants because it may also appear in emission in long-period variable stars (usually late-type AGB stars) in certain phases owing to shock fronts (Lançon & Wood 2000). In Fig. 7, we show individual example spectra for different types of C stars, easily

Table 2. Spectroscopic and photometric catalogue of stars observed in the direction towards NGC 6822. This is part of the full table, which is available in the electronic version of the paper.

ID	X [px]	Y [px]	RA [deg]	DEC [deg]	r [deg]	R [mag]	J [mag]	H [mag]	K [mag]	Sp. Cl. photometry	Sp. Cl. spectroscopy	Quality flag
94208	219.732	1679.789	296.349976	−14.828187	0.1121527	19.772	17.877	17.045	16.898	M	M1III	4
94979	330.734	1801.989	296.357117	−14.834526	0.1206048	19.510	17.528	16.720	16.515	Mca	M1III	4
96968	608.073	1462.465	296.337067	−14.850516	0.1073543	18.978	16.924	16.080	15.693	C	C5.5	5
97590	696.476	1751.644	296.354126	−14.855531	0.1249199	19.406	17.334	16.521	16.218	M	C5.5	5
99641	1001.033	2013.256	296.369537	−14.872893	0.1464667	20.196	17.025	15.971	15.317	C	C6.5	5
101911	1355.722	158.286	296.260742	−14.892557	0.09137722	20.645	17.952	17.153	16.985	M	M	4
77311	48.431	1099.388	296.316101	−14.679276	0.1453135	19.438	17.443	16.601	16.179	C	C6.5	5
79509	475.349	2029.313	296.371155	−14.703938	0.1641518	20.219	18.079	17.198	16.991	M	M1III	5
83906	1226.993	1566.500	296.343781	−14.746560	0.1178242	21.667	17.437	16.532	16.128	C	C5.5	5
85530	1462.654	1902.611	296.363739	−14.759742	0.1306686	23.344	16.528	15.565	14.986	C	C5.5	5
85885	1506.260	2089.456	296.374664	−14.762603	0.1401522	22.981	17.504	16.586	16.355	M	M4III	5
88539	1880.543	1058.628	296.313934	−14.783896	0.07590062	22.971	17.388	16.359	15.668	C	C5.5	4
77230	140.325	1975.243	296.193542	−14.678253	0.1337262	20.206	17.488	16.498	16.071	C	C5.5	5
78095	311.616	1734.144	296.179352	−14.688039	0.1306334	19.813	17.241	16.350	16.076	M	C5.5	5
78871	459.932	2256.131	296.210236	−14.696464	0.1111891	21.556	16.949	16.337	15.919	M	dM5e	5
79224	532.454	1875.599	296.187653	−14.700607	0.1156495	21.826	17.792	17.073	16.777	M	M6.5III	5
79511	589.745	1521.752	296.166718	−14.703956	0.1239035	20.233	17.724	16.890	16.697	M	M1III	4
80764	832.120	1828.010	296.184784	−14.717754	0.1022478	20.280	17.435	16.459	16.039	C	C5.5	5
81015	879.108	1219.159	296.148743	−14.720551	0.1237123	20.331	18.060	17.254	17.066	M	M1III	5
81290	923.831	1041.148	296.138214	−14.723130	0.130111	20.327	17.227	16.188	15.542	C	C6.5	5
82246	1076.064	1643.366	296.173828	−14.731837	0.09789109	20.061	17.335	16.543	16.299	M	M4III	6
83467	1267.180	2155.227	296.204193	−14.742633	0.07085879	18.691	15.048	14.173	13.874	M	M6III	6
83752	1310.298	1599.732	296.171265	−14.745203	0.09053338	20.500	18.020	17.228	16.970	M	C5.5	5
84020	1354.477	1830.278	296.185242	−14.747572	0.07863506	23.015	17.622	16.799	16.588	M	dM	5
85975	1628.458	2046.414	296.197662	−14.763362	0.0587216	20.414	17.175	16.255	15.536	C	C5.5	5
86798	1753.719	2238.658	296.208893	−14.769947	0.04610623	24.466	17.025	16.201	15.758	C	C6.5	5
88152	1934.647	2076.698	296.199615	−14.780900	0.04676038	20.389	18.414	17.421	17.201	C	M2III	5
88716	2021.618	2204.011	296.206879	−14.785284	0.03828439	19.733	18.082	17.209	17.074	M	C5.5	5
93532	99.508	1716.032	296.178833	−14.822721	0.06469996	20.139	17.330	16.475	16.210	M	SIII	5
93858	143.567	1738.309	296.180084	−14.825297	0.0643363	19.755	17.231	16.366	15.897	C	C5.5	6
94446	230.224	2278.535	296.212219	−14.830112	0.03894694	20.872	17.270	16.343	16.036	Cca	C8.2	5
94947	300.292	1631.935	296.173828	−14.834276	0.07354362	20.655	18.015	17.151	16.987	Mca	M1III	5
95293	347.628	1413.000	296.160797	−14.836968	0.08655488	20.626	18.027	17.370	17.092	Mca	dM3	6
73508[1]	1469.541	1550.219	296.488861	−14.638191	0.2982319	20.405	17.496	16.557	15.974	C	C6.5 v	5
68214[1]	636.571	1798.562	296.329102	−14.584000	0.2366088	19.231	17.611	16.957	16.665	M	M5 III e v	5
101802[2]	1328.222	1947.256	296.365631	−14.891643	0.1530257	17.818	15.562	14.7120	14.318	C	M5III	6
100545[3]	1120.211	656.699	296.116089	−14.881053	0.146717	20.608	17.310	16.2500	15.450	C	C5.5	6
86680[3]	1308.239	1484.110	296.014832	−14.769041	0.2283621	18.537	17.050	15.8860	15.051	C	C8.2	5
111590[3]	852.096	1197.049	295.993561	−14.990264	0.3097264	19.735	17.874	16.7020	15.840	C	C6.5	5

Notes. [(1)] LPV defined in Battinelli & Demers (2011). [(2)] IR spectrum from Groenewegen (2004) is available for this star. [(3)] C stars in common with the catalogue of Demers et al. (2006a).

distinguishable by means of the many CN and C_2 bands and an example of a rare S-type star clearly showing ZrO bands. We also plot the spectrum of a similar galactic S star from the atlas of Otto et al. (2011) over our example for comparison. Two figures showing separately the full sample of different subtypes giant and dwarf average spectra are available in the electronic version of the paper.

In total, we determined spectral types for 511 of the 546 spectra with quality flags of 4, 5, or 6 (Table 3). The majority turned out to be foreground dwarfs. This is in part because the colour criterion for the selection of AGB stars in NGC 6822 was on purpose quite relaxed ($(J-K)_0 > 0.74$ mag) to allow the selection also of early-type M stars. In addition, if there was any remaining space in the masks after the primary targets were allocated to slits, then secondary targets, most of which were foreground dwarfs, were also targeted. Among the AGB stars belonging to NGC 6822, the majority are carbon-rich giants. Once again, this partly reflects the selection criteria, which were biased towards the AGB stars and in particular C-rich giants.

Battinelli et al. (2006) mapped the elliptical spheroid of NGC 6822 out to a semi-major axis distance of 36′. In Fig. 8, we show the spatial distribution of spectroscopically observed AGB stars in NGC 6822, as well as the Milky Way dwarfs, for which we have spectra of good quality. Essentially all giants identified by us as having either M-type or C-type AGB spectra are found within the ellipse, and the targets outside this region have been systematically found to have spectral features typical of dwarf stars.

Table 3. Statistics of the spectral classification for the different fields.

Field	All stars	M III	C III	S III	dwarfs	Unclass.
CF	138	55	64	4	8	7
NW1	47	7	10	0	28	2
NE1	96	22	25	1	39	9
SE1	115	24	36	2	48	5
SW1	62	14	16	2	29	1
NE2	70	0	0	0	62	8
SW2	18	1	0	0	14	3
All	546	123	151	9	228	35

Battinelli & Demers (2011) published a catalogue of 63 long-period variable stars (LPVs) in NGC 6822. Cross-correlating our spectroscopic sample with their catalogue, we found two exact matches - a C giant (ID 73508), which is an irregular variable, and an M giant semi-regular variable (ID 68214) with a 149-day period. The latter shows Hα line in emission. Another four variable sources were found within 10″ of our C and S stars, but without more information about the astrometric accuracy of the catalogue, we are unable to exclude that these are spurious matches and therefore do not report them

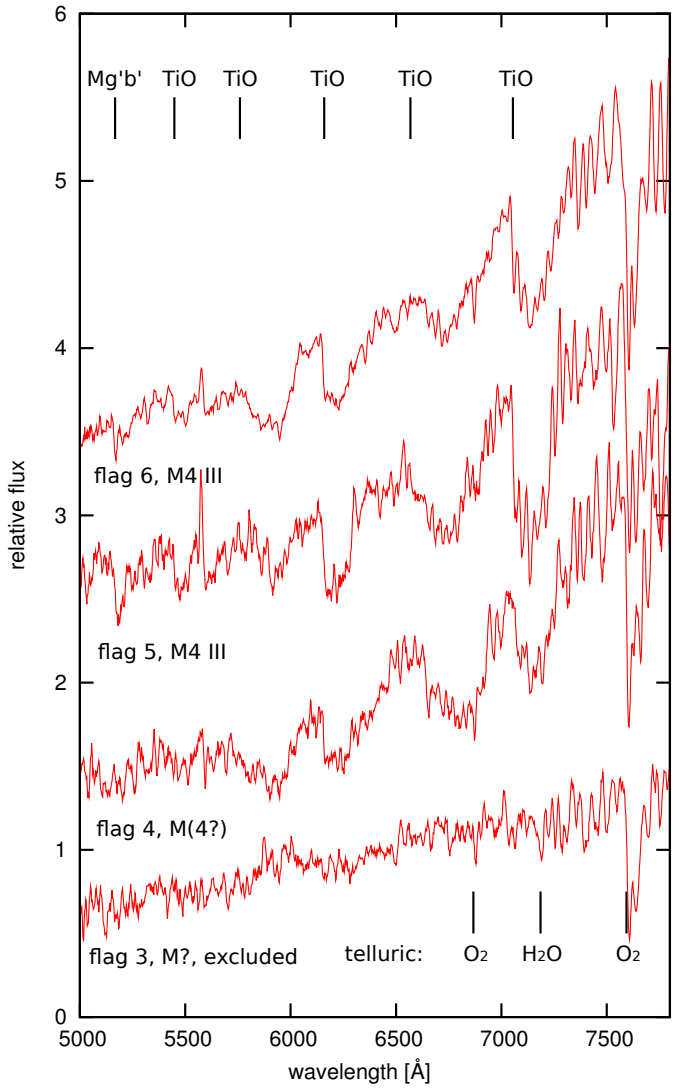

Fig. 3. Example of individual spectra with different quality flags. The spectra are rescaled, shifted along the y-axis by an arbitrary constant for presentation purpose, and smoothed with a level 5 boxcar function.

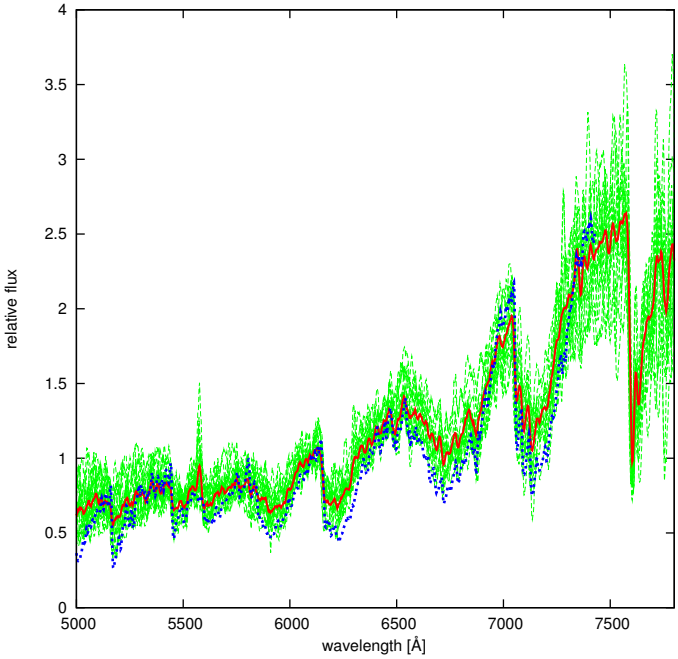

Fig. 4. All spectra classified as M4 III are rescaled and plotted together with green lines. An average M4 III spectrum is calculated and shown in red and a reference M4 III spectrum from the library of Jacoby et al. (1984) is drawn with a blue dotted line.

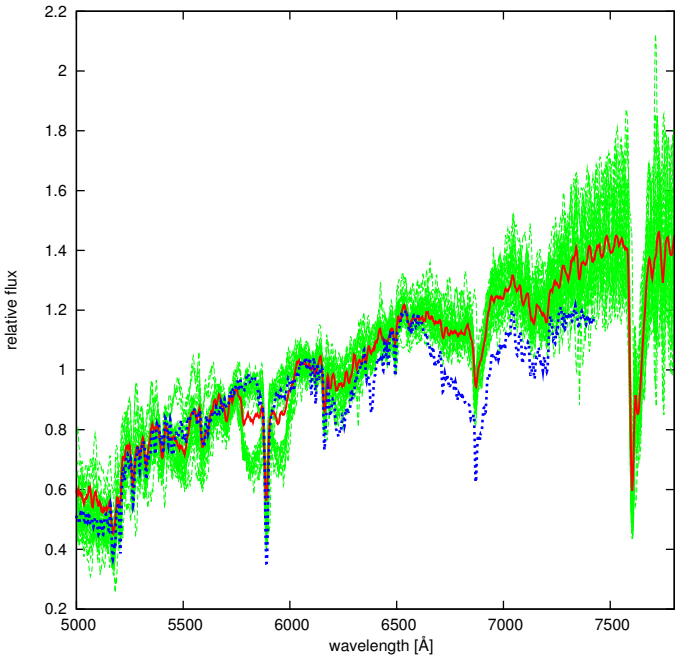

Fig. 5. Same as Fig. 4 but for M0 V spectral class.

here. We also matched our catalogue with the 10 IR spectra obtained by Groenewegen et al. (2009) in NGC 6822. We found two exact matches with their targeted stars, one of which they actually observed (2MASS19452775-1453299) and we confirm that it is an M-type AGB star. Finally, we matched our catalogue with the catalogue of carbon stars (142 sources) obtained by Demers et al. (2006a). We found three exact matches, which were all confirmed as C-type stars based on our spectra. These have the following IDs in Demers et al. (2006a) catalogue: 1075, 1031, and 1026. Details about the stars in common with the cited catalogues are presented at the bottom of Table 2 marked with different indices. All stars that were matched based on coordinates with AGB samples of other authors, were also matched in spectral classification.

We emphasize the small overlap between our spectroscopic catalogue and the cited works. This might be partially explained by the limited choice of slit positions on the VIMOS masks. We also cross-correlated our full IR catalogue with these surveys and found that it contains 33 (from 63) sources from Battinelli & Demers (2011), 8 (from 10) sources from Groenewegen et al. (2009), and only 20 (from 142) sources from Demers et al. (2006a). The astrometric differences are less than 0.2″ and the stars in common have similar J and K magnitudes. It is not trivial to answer where the biases in the full catalogue come from but this result might mean that our catalogue suffers from some incompleteness in either the outer regions of the galaxy, the redder part of the CMD, or both. All the stars in Demers et al. (2006a) have colours $J - K > 1.5$ mag and are situated outside the central parts of NGC 6822. Other reasons could be the different criteria for selecting stellar sources or larger astrometry errors.

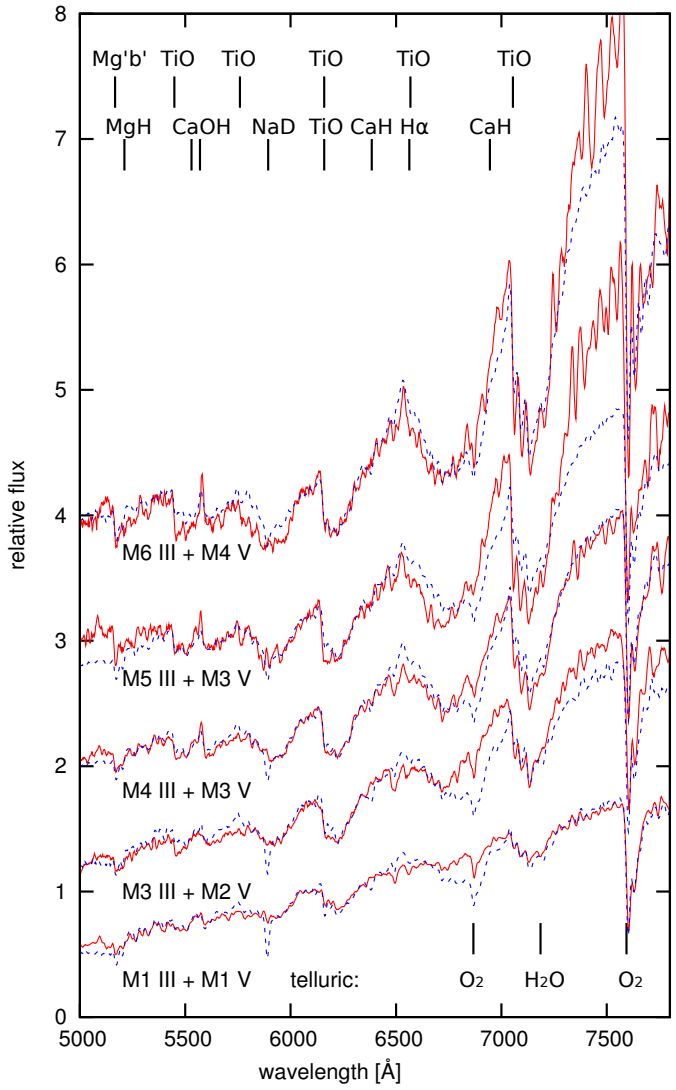

Fig. 6. Comparison between average dwarf and giant stars spectra with similar spectral class. The similarities of the two types of spectra increase with increasing the spectral type. The spectra of giants are presented in red and the dwarfs with blue dotted lines. The positions of some of the most characteristic features (upper row for giants, second row for dwarfs) as well as some telluric bands (in the bottom) are shown with black lines. The spectra are shifted along the y-axis with an arbitrary constant for presentation purpose.

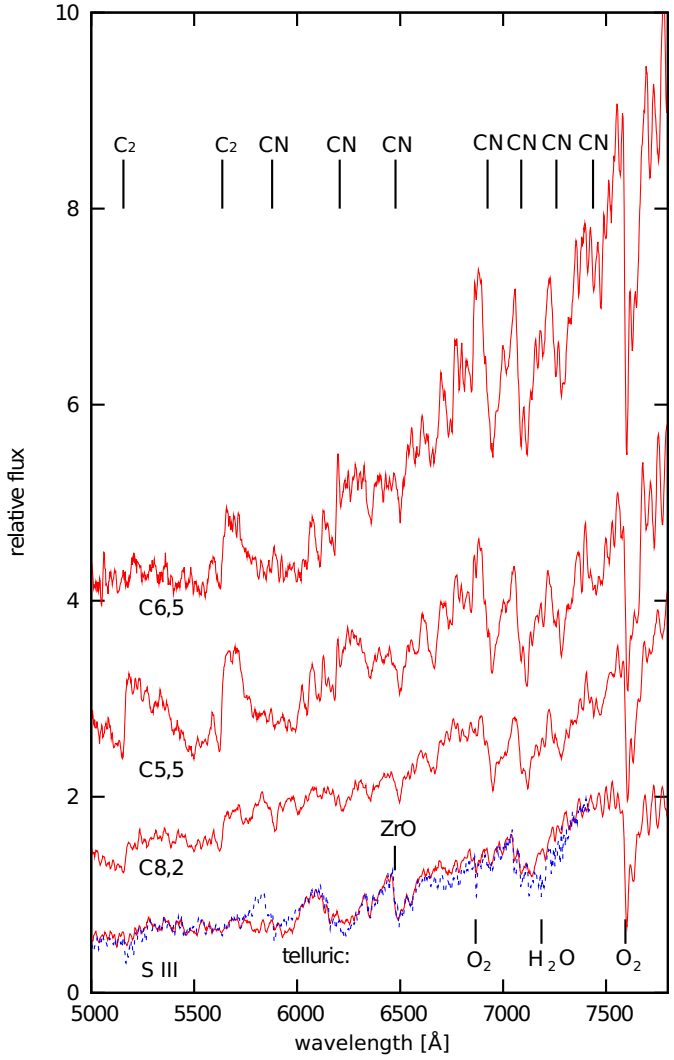

Fig. 7. Example spectra of individual stars of different C-types and one S-type plotted together. A spectrum of a similar star from the atlas of S stars (Otto et al. 2011) is overplotted with a blue dotted line for comparison. Positions of some of the most typical features are shown with black lines: C_2 and CN bands for the carbon stars and ZrO for the S-type stars. The spectra are shifted along the y-axis by an arbitrary constant for presentation purpose.

4. Results and discussion

4.1. Colour - magnitude and colour - colour diagrams

Fig. 9 shows the $(J-K, K)$ colour-magnitude diagram (CMD) for all stars with good quality spectra. The diagram contains three distinct groups of objects - the two different types of AGB stars and the foreground population. They are depicted with different colour codes according to our spectral classification. We note that most of the M-type AGB stars have a colour index that is typically bluer than the $(J-K)_0 = 1.2$ mag limit (Sibbons et al. 2010). The C-type stars, however, are dispersed across both sides of this limit. It is interesting that the bluer C-type stars, as well as the S-type stars are distributed preferably over the brighter end of the M star sequence. The foreground stars are distributed in a vertical sequence of $(J-K)_0 \sim 0.8$ mag, that is easily

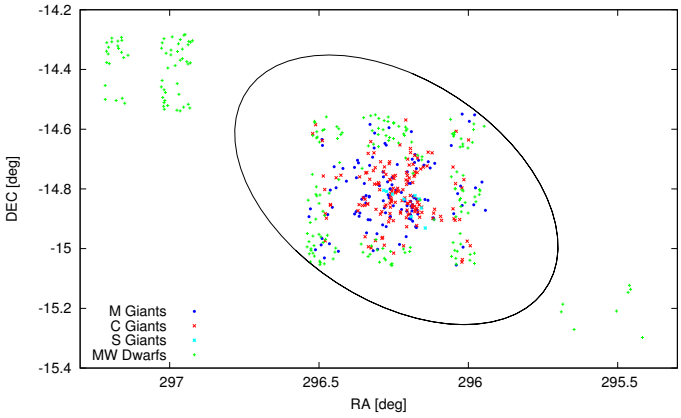

Fig. 8. Spatial distribution of all stars with acquired spectra of good quality. The outer 36′ ellipse (Battinelli et al. 2006) is shown with solid black line. North is up and east is to the left.

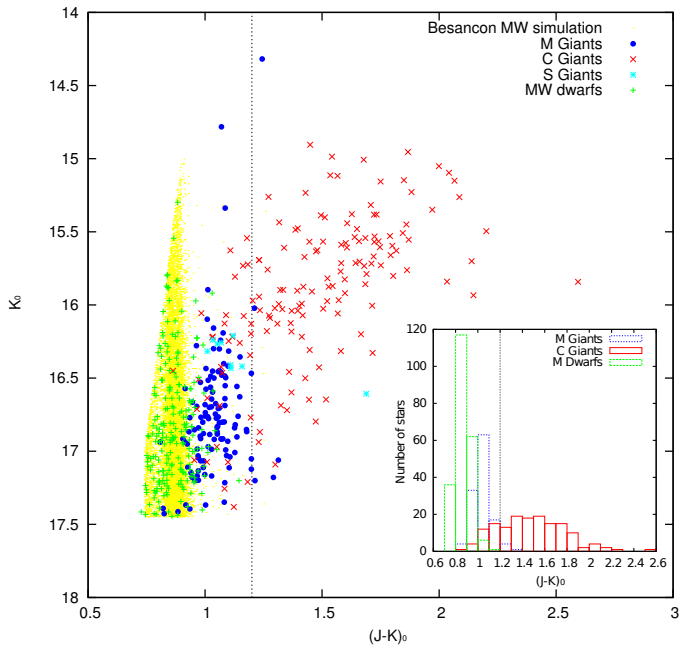

Fig. 9. CMD for all stars in the field of NGC 6822 with good quality spectra. The black dotted line shows the photometric selection criterion for differentiating between C- and M-type giants from Sibbons et al. (2010). The Milky Way dwarf sequence can be easily distinguished, even though it overlaps with the AGB sequence. The simulation of the foreground population obtained with the Besançon models is indicated by yellow dots. The smaller rectangle is a histogram of this CMD.

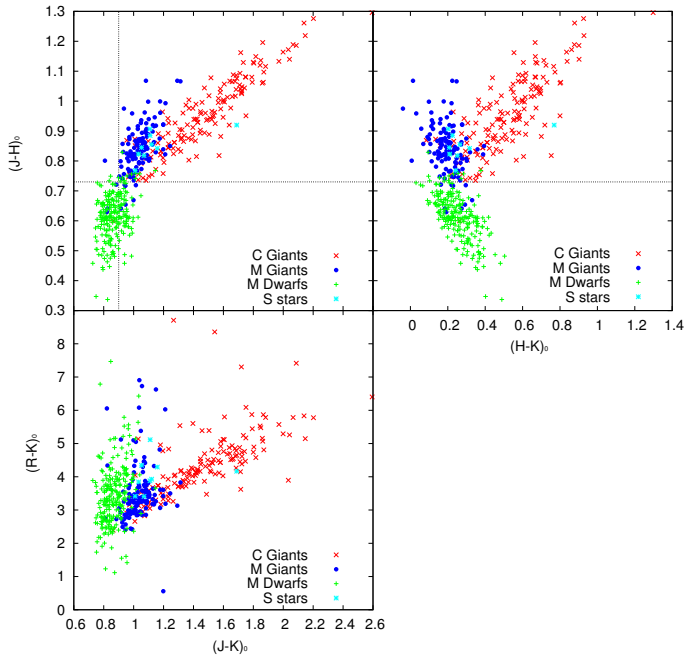

Fig. 10. Two-colour diagrams. Upper-left: $(J-K,\ J-H)$ two-colour diagram. The two dotted lines show the AGB selection criteria: $(J-H)_0 > 0.73$ mag and $(J-K)_0 > 0.9$ mag; Upper-right: $(H-K,\ J-H)$ two-colour diagram. The NGC 6822 carbon- and oxygen-rich AGB stars can be more clearly separated in this diagram; Bottom-left: $(J-K,\ R-K)$ two-colour diagram.

distinguishable but has a significant overlap with the AGB star distribution. This can be seen more easily in the histogram in Fig. 9. The histogram presents the number of classified stars vs. the $(J-K)_0$ colour index in 0.1 magnitude bins. Most of the foreground Milky Way dwarfs have $(J-K)_0$ colours between 0.7 and 1.0 mag, with maximum number of dwarfs beeing in the 0.8 – 0.9 mag bin. Most of the M giant stars are in the 1.0 – 1.1 mag bin and they strongly overlap with the dwarf sequence for the range $(J-K)_0 \sim 0.9 - 1.0$ mag.

We used the Besançon model of the Milky Way (Robin et al. 2003) to simulate the foreground population. The model simulated about 11000 M- and K-type main sequence stars in total, within an area of 1.14 deg^2 centred on the centre of NGC 6822. The model parameters are chosen so that all simulated stars match the cuts of the full IR catalogue. The simulation agrees very well with the positions of the stars classified as dwarfs on the CMD. The simulated stars are shown with small yellow dots in Fig. 9. The Besançon model predicts roughly ∼ 10000 dwarfs per deg^2, while in the full UKIRT catalogue the density of stars is ∼ 7000 stars per deg^2, the large majority of which are dwarfs (∼ 6000 per deg^2).

Fig. 10 shows three two-colour diagrams. The $(H-K,\ J-H)$ diagram (upper-right) is a powerful tool for separating the foreground Milky Way dwarfs and also allows a separation between the oxygen- and carbon-rich AGB stars (Aaronson & Mould 1985; Bessell & Brett 1988). In general AGB stars are expected to have $(J-H)_0 > 0.73$ mag and all foreground dwarf stars should be bluer than this limit (Gullieuszik et al. 2008; Sibbons et al. 2010). Our spectra show that this is true for all spectroscopically observed stars with few exceptions. We find that the giants bluer than the $(J-H)_0 = 0.73$ mag limit are mostly early M-type giants and only one is a C-type giant. There is one dwarf star, which lies significantly redward of the colour limit at $(J-H)_0 = 0.82$ mag. There is also a possibility that, owing to the high density of stars, few slits captured the light from neighbouring dwarf stars that were not the main target. We found this to be the case for one photometrically classified C-type star, which was targeted in two masks. In the spectrum from the first mask, we can clearly see a carbon-rich star and in the spectrum from the second mask, a foreground K dwarf. We excluded the spectra of four dwarf stars, which had been photometrically classified as carbon rich-stars, because of this effect. In the $(J-K,\ J-H)$ two-colour diagram (upper-left), the C- and M-type giants are more intermixed but it shows our selection criteria for AGB stars. The horizontal line at $(J-H)_0 = 0.73$ mag separates the foreground from NGC 6822 stars, and the vertical line at $(J-K)_0 = 0.9$ mag indicates the blue limit for the AGB stars.

We also present the $(J-K,\ R-K)$ two-colour diagram (bottom-left) in Fig. 10. It shows a clear separation between the different types of stars, which is however not as clean as for the IR photometry. This is mostly due to the larger R-band photometry errors and the probable variability of the targeted AGB stars (for which IR and R-band photometry were taken in different epochs), which would smear out their locations in the two-colour diagram. Otto et al. (2011) indicate that S-type stars are more clearly separated in this visible-IR two-colour diagram, which is also the case here. The colours of the Galactic S stars from Otto et al. (2011) are similar to the colours of S stars in NGC 6822.

4.2. Photometric criteria for C vs. M giants selection based on the spectroscopic sample

On the basis of our spectroscopic sample, we derive new photometric selection criteria for distinguishing between different

Table 4. AGB stars selection from the photometric catalogue.

Criterion	M III	C III	S III	dwarfs
$(J-H)_0 > 0.72$	93%	99%	100%	9%
$(J-H)_0 > 0.73$	93%	99%	100%	6%
$(J-H)_0 > 0.74$	92%	98%	100%	5%
$(J-H)_0 > 0.75$	88%	96%	100%	3%
$(J-H)_0 > 0.73$ and $(J-K)_0 > 0.90$	92%	99%	100%	5%

types of AGB stars in NGC 6822 and foreground population. As already mentioned, the photometry is based on the near-IR catalogue of Sibbons et al. (2010). The selected photometric sample includes over 21000 stars found within a radius of 1 degree from the centre of NGC 6822, that are brighter than $K_0 = 17.45$ mag in accordance with the value for the TRGB of NGC 6822 from Sibbons et al. (2010).

We find that the easiest way to differentiate between the AGB population of NGC 6822 and the foreground dwarfs is to use these two-colour diagrams. We tested several $(J-H)_0$ cuts, and our results are summarized in Table 4. This table indicates the percentage of spectroscopically confirmed AGB stars that would be identified as AGB stars using a certain cut in $(J-H)_0$. We note that our spectroscopic sample contains almost no stars with the colours $(J-H)_0 > 0.73$ mag and $(J-K)_0 < 0.9$ mag (Fig. 10 upper-left diagram). These represent about 3% of the whole photometric sample, and because we are unable to determine their type, we exclude them. In this work, we use $(J-H)_0 > 0.73$ mag and $(J-K)_0 > 0.9$ mag to select AGB stars and $(J-H)_0 < 0.73$ mag to select foreground stars. After applying these cuts, we found that our photometric sample includes about 2800 AGB candidates.

We propose two different approaches for distinguishing between carbon- and oxygen-rich AGB stars from the $(J-K,\ K)$ CMD in order to estimate the C/M ratio. As we mentioned before, almost all S-type stars (8 of 9) and most of the C-type stars with colours $(J-K)_0 < 1.2$ mag are brighter than $K_0 = 16.45$ mag. We can also see that there are roughly equal numbers of M- and C-type stars in the region $(J-K)_0 < 1.2$ mag and $K_0 < 16.45$ mag according to our spectroscopic sample: 17 M-type and 18 C-type stars. Our first set of selection criteria (Fig. 11) is based on this result. We exclude all objects for which $(J-K)_0 < 1.2$ mag and $K_0 < 16.45$ mag. This permits us to remove the S-type stars as well as the region in the CMD where the C- and M-type stars strongly overlap but have a number ratio close to 1. We then simply divide the CMD into two parts: stars bluer than $(J-K)_0 = 1.2$ mag, which we call M giants, and redder than $(J-K)_0 = 1.2$, which are C giants. If we adopt a distance modulus of 23.35 mag (weighted average obtained from Tables 4 and 5 in Gorski et al. (2011)), the absolute K magnitude of this limit will be $M_K = -6.90$ mag.

The second approach is also based on cuts in the $(J-K,\ K)$ CMD. We assume that all objects with $(J-K)_0 < 1.2$ mag and $K_0 > 2\times(J-K)_0 + 14.05$ are M-type giants and objects with $K_0 < 2\times(J-K)_0 + 14.05$ and $K_0 > -2\times(J-K)_0 + 17.65$ are C-type giants (Fig. 12). This method provides the clearest possible separation between carbon- and oxygen-rich AGB stars but does not account for S-type stars. The excluded regions contain only 6% of the AGB candidates and the upper region might consist mostly of supergiants and foreground stars. In the fainter excluded region, we have three spectroscopically confirmed M giants and three C giants. Although we recognize the effect of small number statistics, there appears to be a large overlap between the C- and M-type stars in this region of the CMD. Adopting a distance modulus of 23.35 mag, and correcting for it, the selection criteria are all objects with $(J-K)_0 < 1.2$ mag and $M_K > 2\times(J-K)_0 - 9.30$ are M-type giants and objects with $M_K < 2\times(J-K)_0 - 9.30$ and $M_K > -2\times(J-K)_0 - 5.70$ are C-type giants.

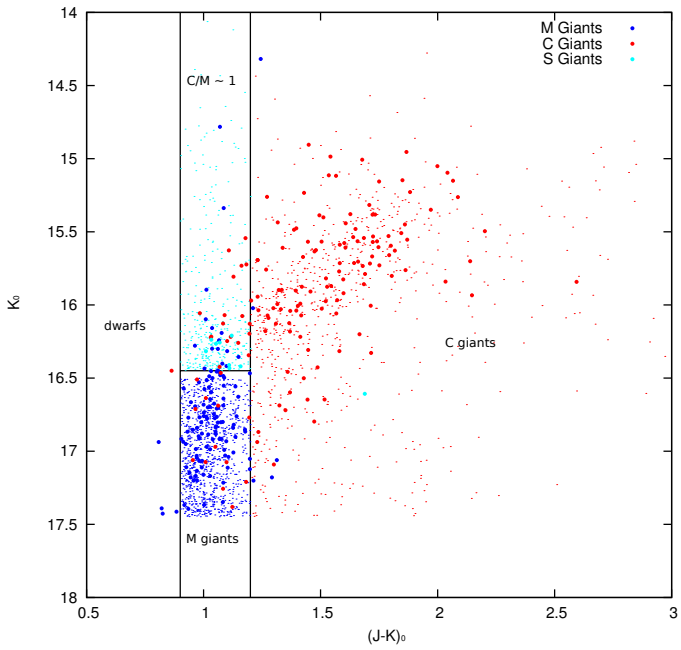

Fig. 11. First C- and M-type set of selection criteria. Most of the S-type stars and an equal number of C- and M-type stars are found in the region $K_0 < 16.45$ mag, $(J-K)_0 < 1.2$ mag. Excluding this region, our selection is based on a colour cut at $(J-K)_0 = 1.2$ mag. The photometric sample is presented with dots and the spectroscopically confirmed stars with larger points.

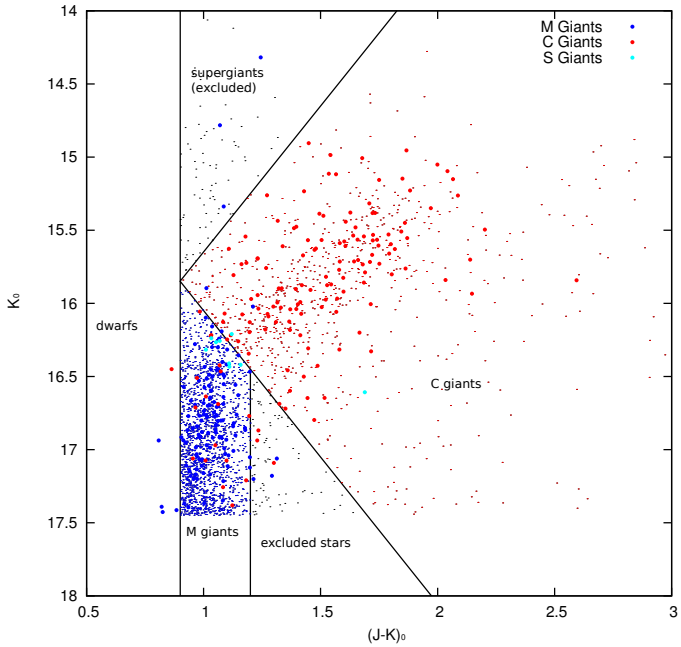

Fig. 12. Second C- and M-type set of selection criteria. The two excluded regions contain only 6% of the AGB candidates. The photometric sample is presented with dots and the spectroscopically confirmed stars with larger points.

Table 5. Results of the C- and M-type star selection criteria.

I set criteria:	M-type sel.	C-type sel.	Excluded
Sp. M-type	74% + (14%)	4%	(14%)
Sp. C-type	9%	79% + (12%)	(12%)
Sp. S-type	0%	11%	89%
II set criteria:			
Sp. M-type	84%	2%	6%
Sp. C-type	11%	86%	2%
Sp. S-type	78%	22%	0%

Table 6. Expected contamination by different types of stars in the selection boxes.

I set criteria:	M-type selection	C-type selection
M-type cont.	79%	4%
C-type cont.	11%	95%
S-type cont.	0%	1%
dwarfs cont.	10%	0%
II set criteria:		
M-type cont.	75%	2%
C-type cont.	12%	97%
S-type cont.	5%	1%
dwarfs cont.	8%	0%

Tables 5 and 6 present the statistics of our selection criteria. In particular, Table 5 illustrates the effectiveness of both selection criteria. It lists the percentage of all spectroscopically classified stars for each spectroscopic class (e.g. M III, C III, S III) that coincides with the various photometric selection boxes (M-type selection, C-type selection, excluded). Table 6 instead shows the expected contamination of the M-type and C-type photometric selection boxes. This is estimated by assuming that the total number of spectroscopically confirmed stars in a given selection box (e.g. M-type selection or C-type selection box) is 100% and then computing the percentage of M-type, C-type, S-type, or dwarfs in that sample. We refer to this table when we discuss the overall C/M ratio in Sect. 4.3. The two selection criteria are good for the purpose of deriving the C/M ratio because some regions of the CMD, with reciprocal contamination, are excluded. They cannot be used to obtain the absolute number of C- and M-type stars in the galaxy.

4.3. C/M ratio and metallicity distribution

Fig. 13 shows the number density of sources with good quality spectra. We counted the stars of a given spectral type in 18×18 bins, where a single bin corresponds to $2.0' \times 1.8'$ rectangle ($36' \times 20'$ field). The source density in each map is smoothed with a boxcar function of $width = 2$ prior to the construction of the greyscale images, where higher concentrations of sources are indicated with darker regions. From left to right, we show all stars, all AGB stars, and the foreground stars in the first row, and M-type AGB stars, C-type AGB stars, and the C/M ratio map in the second row. The size of the maps corresponds to the observed field within the outer ellipse of NGC 6822 according to Fig. 8 and is based on 271 AGB stars in total: 121 M- and 150 C-type giants. The number of individual stars is smaller than the number of obtained spectra because few stars were targeted in two of our masks. We can see from Fig. 13 that the AGB population is concentrated at the centre of the galaxy. However the large C/M ratio in the central parts (which varies between 1 and 2) is due to underestimating the number of M stars with respect to the C stars and it is possible that the small C/M ratio in the outer parts is due to small number statistics. These maps reflect the biases in the spectroscopic sample (C stars were targeted preferentially) and cannot be used to derive the metallicity distribution within the galaxy.

To investigate the C/M ratio and metallicity distribution within NGC 6822, we use the complete near-IR photometric catalogue. Here we apply the second set of photometric selection criteria (discussed in the previous section) to distinguish between carbon- and oxygen-rich AGB stars. We obtain very similar results when the first set of criteria is used. The results are presented in Fig. 14, which is almost identical to Fig. 13 but the stars are binned in 36×36 bins, of $1' \times 0.9'$ each. The map is based on 1753 AGB stars in total, 970 and 783 photometrically classified M- and C-type stars, respectively. We would expect the foreground density map to be flat but we can see some overdensity of stars at the centre coinciding with the galaxy. This means that we underestimate the number of AGB stars, which are most probably M-type giants. This overdensity is quite small, only $1.3\,\sigma$ over the foreground fluctuations and has no significant effect on our C/M ratio estimate.

The overall C/M ratio is 0.8 according to the number of stars in the selection boxes. However, if we take into account the expected contaminations in the selection boxes from Table 6, i.e. the number of M giants to be 75% of the number of stars in the M-type selection box plus 2% of the number of stars in the C-type selection box plus 4% from the dwarfs selection and the number of C giants to be 97% of the C-type selection plus 12% of the M-type selection, we calculate a C/M ratio $\sim$ 1.05. This value is in excellent agreement with C/M ratio of 1.0 obtained by Letarte et al. (2002).

We see a similar trend in the C/M ratio distribution across the galaxy as described by Cioni & Habing (2005). The galaxy centre has a relatively small C/M ratio that increases when moving outwards. The maximum of the C/M ratio follows a broken ellipse around the galactic centre and then starts to decrease with increasing radii. This decrease in the C/M ratio towards the outer regions may be real or due to small number of statistics. A bar-like structure traced by younger stars in Gouliermis et al. (2010) cannot be distinguished in the C/M ratio distribution. The area investigated by Karampelas et al. (2009) corresponds to the field of Fig. 14. Beyond that, the density of stars is too low and it is difficult to estimate the C/M ratio. We discuss the stellar density in the outermost regions of our photometric catalogue in Sect. 4.5.

The variation in the C/M ratio across the face of the galaxy can be explained by a variation in the metallicity. A higher C/M ratio relates to a lower metallicity. This relation is well-studied in previous works of Cioni & Habing (2003, 2005) for the SMC, LMC, M 33, and this galaxy, and calibrations between C/M and [Fe/H] were presented in Groenewegen (2004), Battinelli & Demers (2005), and Cioni (2009). The physical reasons for this correlation are explained by Scalo & Miller (1981) and Iben & Renzini (1983): (i) O-rich AGB stars of lower metallicity turn more easily into C-rich stars; (ii) evolutionary tracks for lower metallicities correspond to higher temperatures; (iii) in very low metallicity environments, post-horizontal branch stars may fail to become AGB stars.

In our study of NGC 6822, the C/M ratio varies between 0.2 and 1.8 according to Fig. 14 and this corresponds to a metallicity variation of Δ[Fe/H] $\sim$ 0.4 dex (between -0.9 dex and

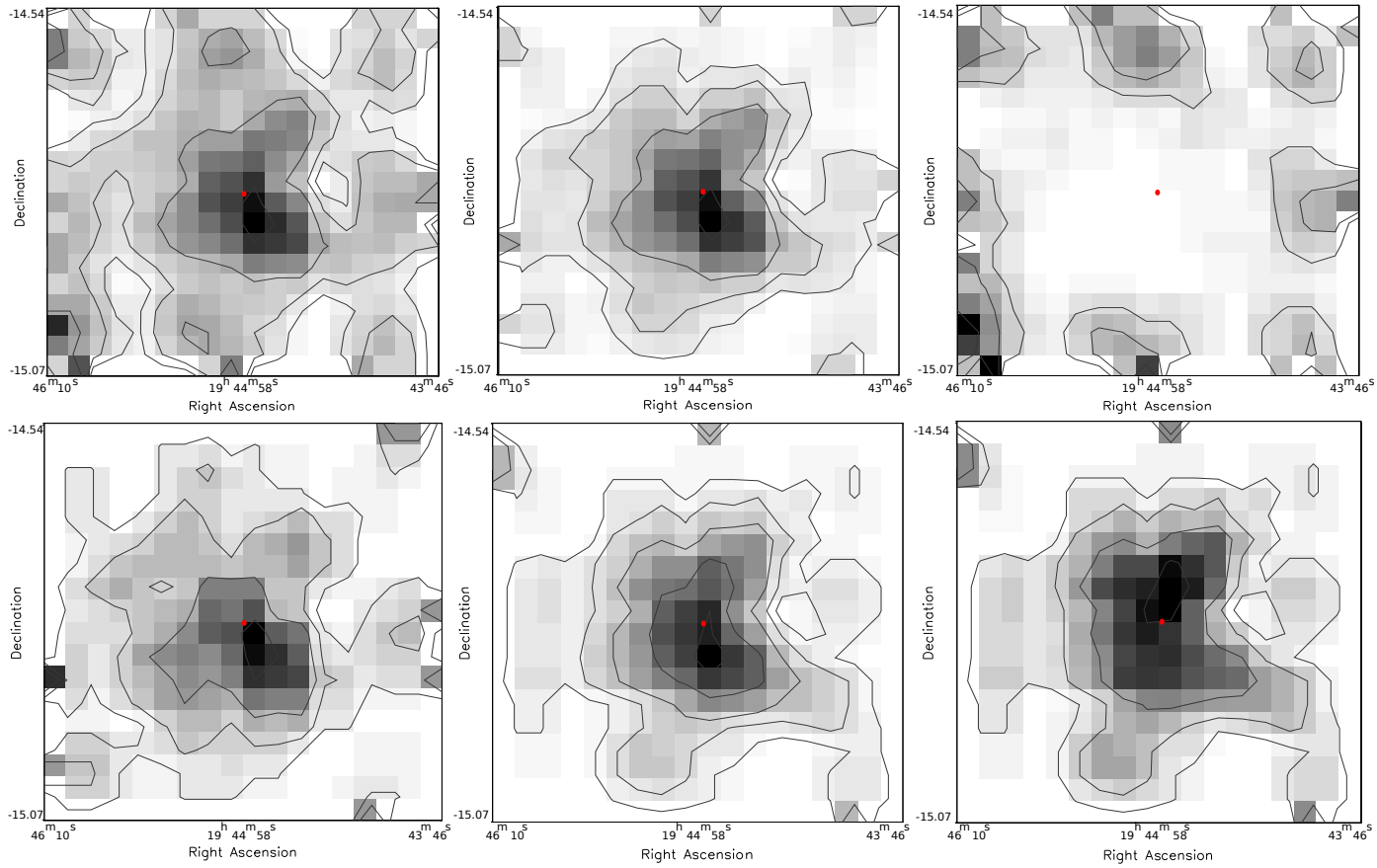

Fig. 13. Logarithmic and smoothed density distributions of all stars with good quality spectra. The maps are in 18×18 bins 2.0′×1.8′ each as follows; top: all stars, all AGB stars, and all dwarf stars (contours are for 0.5, 1, 2, 5 density levels); bottom: M-type AGB stars, C-type AGB stars (contours are for 0.2, 0.5, 1, 2, 3 density levels), and C/M ratio map (contours are for ratios 0.2, 0.5, 1, 2). Darker regions correspond to higher density. The centre of the galaxy is indicated with a small red dot. North is up and east is to the left.

−1.3 dex) with an average [Fe/H] ∼ −1.2 dex using the calibration proposed by Groenewegen (2004)

$$[\mathrm{Fe/H}] = -0.42 \times \log(\mathrm{C/M}) - 1.23. \quad (3)$$

Another calibration proposed by Battinelli & Demers (2005) is

$$[\mathrm{Fe/H}] = -0.59 \times \log(\mathrm{C/M}) - 1.32. \quad (4)$$

Using this we obtain an average value of [Fe/H] ∼ −1.3 dex with a spread of between −0.9 dex and −1.5 dex. A revision of Eq. 4 is presented in Cioni (2009), who propose the alternative relation

$$[\mathrm{Fe/H}] = -0.47 \times \log(\mathrm{C/M}) - 1.39. \quad (5)$$

For NGC 6822, we get an average value of the [Fe/H] index ∼ −1.3 dex with a spread of between −1.1 dex and −1.5 dex. If we adopt C/M ratio ∼ 1.05, the obtained metallicity values are slightly lower, but still very similar to the [Fe/H] values discussed here. The metallicity estimates are in good agreement with the results of Tolstoy et al. (2001) and Davidge (2003). The former study found an average [Fe/H] = −1.0 ± 0.5 dex with a spread of between −0.5 and −2.0 dex based on Ca II spectroscopic measurements of 23 RGB stars, while the latter derived [Fe/H] = −1.0 ± 0.3 dex from the slope of the RGB. A measurement of the Ca II triplet absorption lines in a statistically significant number of AGB stars in NGC 6822 is the subject of a subsequent paper by our team to provide an independent estimate of the metallicity index.

4.4. C/M ratio and possible age variations

Feast et al. (2010) suggested that radial trends of the C/M ratio across the galaxy might also be explained by age rather than metallicity variations. We test this possibility by fitting isochrones from the Padova library (Marigo et al. 2008; Girardi et al. 2010). The comparison with isochrones shows that the AGB stars are older than 0.8 Gyr but an upper age limit is difficult to establish because the isochrones become uncertain for ages > 2.0 Gyr in this region of the CMD. We compare different regions of high and low C/M ratios in the galaxy with isochrones for ages 1.0 and 1.5 Gyr and metallicities between −0.7 and −1.3 dex. We see that regions with larger ratios have slightly tighter fits by isochrones of age 1.5 Gyr, thus are a bit older than the regions with relatively smaller ratios, which are more consistent with isochrones of age 1.0 Gyr (Fig. 15). The selected regions are marked on the C/M ratio map in Fig. 14: blue for smaller and red for larger ratios. We note, however, that there are a number of uncertainties such as whether there is a significant intrinsic reddening, and any uncertainty in both the distance modulus and the theoretical models themselves, that could bias the conclusions.

In accordance with this line of thought, the slight shift in the peak of the M star distribution with respect to the C stars is unsurprising and probably means that the photometric selection criteria select M stars that are younger than the bulk of C stars. While the densest concentration of C stars is located at the cen-

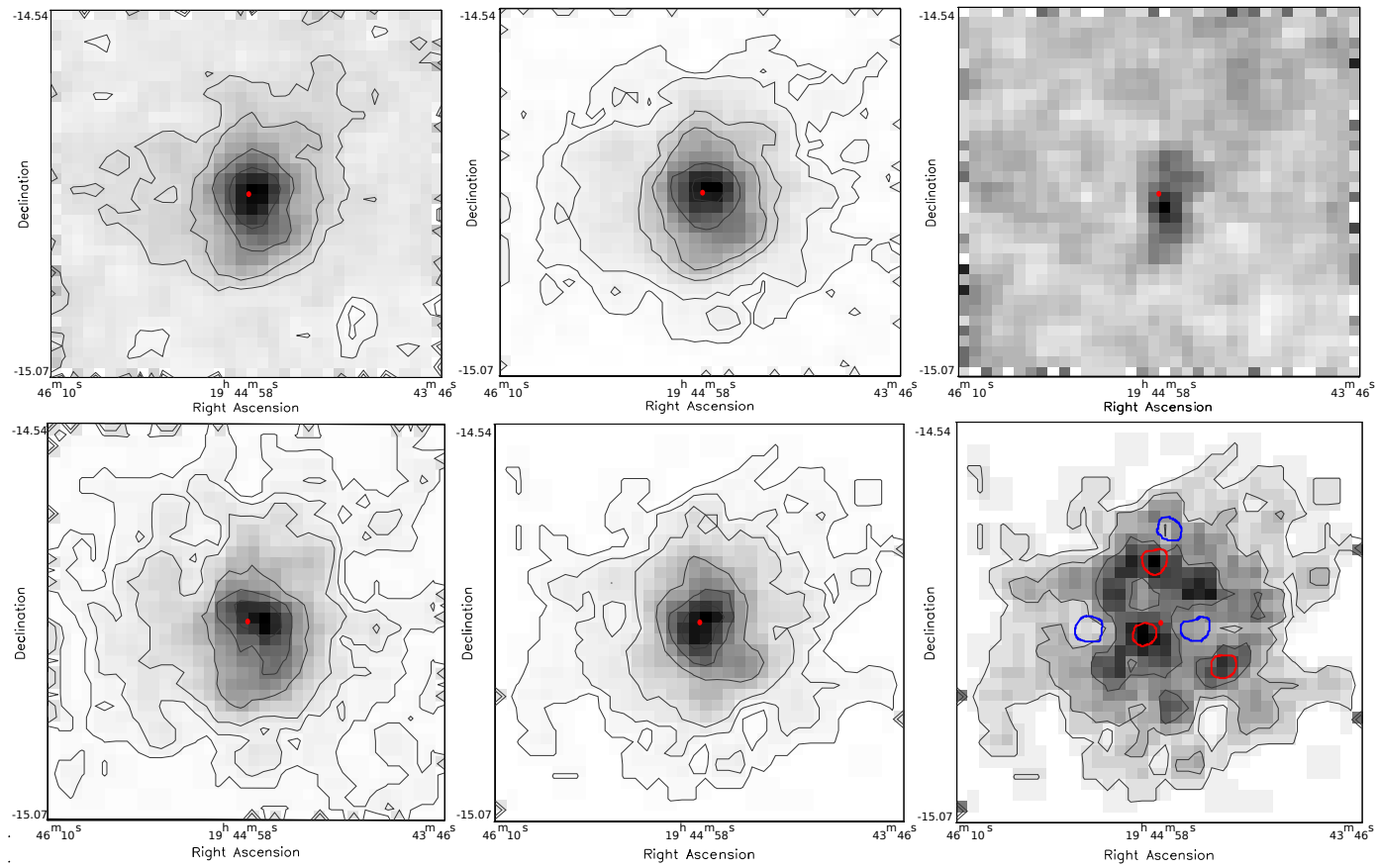

Fig. 14. Logarithmic and smoothed density distributions of the stars from the near-IR catalogue. The maps are in 36 × 36 bins 1.0′ × 0.9′ each as follows; top: all stars, all AGB stars, and all dwarf stars (contours are for 0.5, 1, 3, 5, 10, 15 density levels); bottom: M-type AGB stars, C-type AGB stars (contours are for 0.2, 0.5, 1, 3, 5, 7 density levels), and C/M ratio map (contours are for ratios 0.2, 0.5, 1). Darker regions correspond to higher density. The centre of the galaxy is indicated with a small red dot. The blue circles indicate low and the red circles high C/M regions that are further discussed in Sects. 4.4 and Fig. 15. North is up and east is to the left.

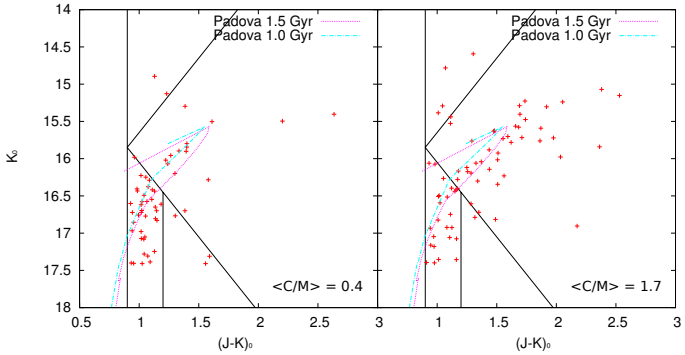

Fig. 15. Stars from three regions of high and low C/M ratios are plotted and compared with isochrones for [Fe/H] = −1.0 dex and ages 1.0 and 1.5 Gyr. The selected regions are indicated in Fig. 14. It seems that larger ratios refer to slightly older ages.

tre of NGC 6822, the M star distribution peaks about 1′ west of it, centred on a bright UV-emission region of recent star formation detected by GALEX (region 26, defined in Efremova et al. (2011)).

4.5. Structure of NGC 6822

The near-IR catalogue covers a region of roughly one degree from the centre of NGC 6822. This allows us to investigate the stellar density of probable galaxy members to this extent. Using the second set of selection criteria, we found that 93% of the photometrically classified C giants and only 64% of the M giants are within the outer ellipse of Battinelli & Demers (2005). We studied the stellar density and the interstellar extinction (using the Schlegel et al. (1998) extinction maps) towards four fields (indicated in Fig. 16 and referred to as NW, SW, NE and SE in Table 7) outside the Battinelli ellipse. We note that a larger number of possible galaxy members extends to the south-west at least one degree from the NGC 6822 centre. The overall stellar density in the south-west field is indeed a little higher than the average foreground density, and the extinction is the same as towards the centre of the galaxy, $E(B-V) = 0.24$ mag.

We see that there is some variation in the extinction between these four fields, which is lower in the north-west and north-east fields, but that this difference corresponds to a $\Delta E(J-H) = 0.02$ mag correction to the $J-H$ colour index, which is the principal means of AGB star selection. Hence, we can assume that the IR extinction in the field of the entire near-IR catalogue is rather constant. In the M III column of Table 7, we list the number of M-type AGB candidates per field assuming a constant $E(B-V) = 0.24$ mag in all fields and in brackets we list

Table 7. Stellar density in four outer fields around NGC 6822, considering only the AGB population ($K < 17.45$ mag).

Field	RA [deg]	Dec [deg]	Radius [deg]	M III count	C III count	Dwarfs count	Fraction of AGB AGB/all	Total st. density [stars p. sq. arcmin]	$E(B-V)$ [mag]
NW	295.794	−14.198	0.2	25 (48)	0	892	0.03	2.028	0.172
SE	296.702	−15.240	0.2	13 (13)	3	848	0.02	1.911	0.226
NE	296.873	−14.338	0.2	31 (43)	2	746	0.04	1.723	0.187
SW	295.620	−15.302	0.2	130 (130)	11	864	0.14	2.223	0.241

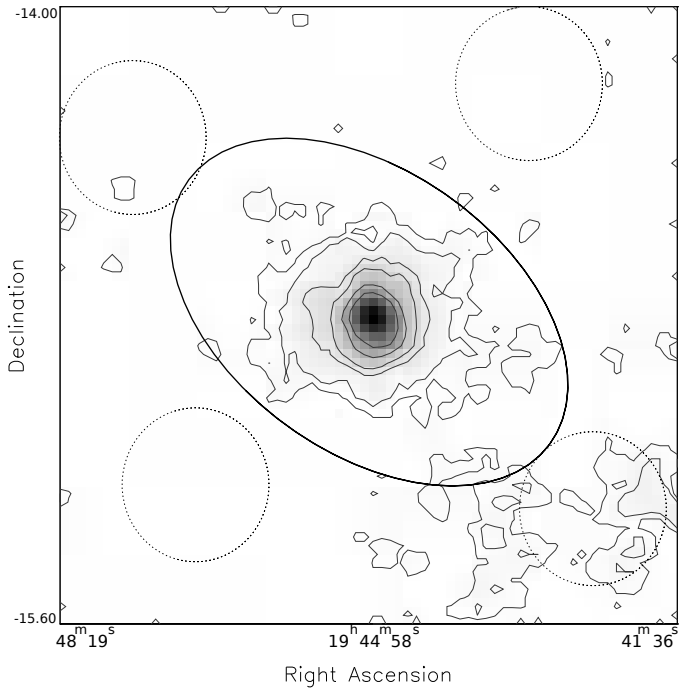

Fig. 16. Smoothed and logarithmic density map of all AGB candidates within the entire field of the IR catalogue. We see a rather significant excess of stars south-west of the centre of the galaxy. The map consists of 72×72 bins, 1.4×1.3 arcmin each. Contours are for 0.5, 1, 3, 5, 10, 15 density levels. The Battinelli & Demers (2005) ellipse and the four discussed outer fields are sketched along. North is up and east is to the left.

the number of M-type AGB candidates that we would have if we adopt the appropriate extinction value from the last column of Table 7. The extinction correction does not lead to any new C-type AGB candidates in the sample but we note that a small correction to the $J-H$ limit could have a significant impact on the number of M-type AGB stars and foreground stars. About 10% of the photometrically recognized galaxy members may actually be foreground dwarfs according to our selection criteria. A logarithmic and smoothed density map of all AGB candidates within the field of the near-IR catalogue is presented in Fig. 16. The isodensity contours that we obtain are very similar to the map presented in Letarte et al. (2002, see their Fig. 9).

We can also consider the full photometric catalogue, which, although not complete, extends to a faintness level of $K_0 = 19$ mag. We adopt $(J-H)_0 > 0.73$ mag to select RGB and AGB candidates (a $J-K$ limit is not adopted because of the expected slope in the RGB) and investigate the stellar densities within the same four outer fields. We again see higher density of possible members of NGC 6822 towards the south-west, although less pronounced because of the unavoidable higher contamination of foreground stars in the selected sample.

Hence, this excess of stars seems to be real but a spectroscopic confirmation of their membership to the galaxy is required.

5. Conclusion

We have presented spectroscopic observations of about 800 stars in the field of the NGC 6822 dwarf galaxy, 511 of which are of good enough quality to permit a reliable spectral classification. The observed stars have been classified as M, C, and S spectral types or foreground dwarfs according to their typical spectral features. We have presented the largest spectroscopic catalogue to date of carbon and oxygen rich AGB stars in NGC 6822. Their distribution in colour-magnitude and colour-colour diagrams was discussed, and we proposed and quantified new photometric selection criteria between the different types of stars. Foreground stars tend to have colours $(J-H)_0 < 0.73$ mag and follow a vertical sequence with a peak at $(J-K)_0 \sim 0.8$ mag on the $(J-K)_0$ vs. K_0 CMD. This was also confirmed by the Besançon Milky Way model (Robin et al. 2003). We found, however, that this model overpredicts the stellar density in the direction of NGC 6822. We also conclude that a small variation in the dwarfs vs. AGB selection criteria may have a significant impact on the number of AGB stars with respect to the foreground.

Our selection of C- and M-types giants was based on selection boxes in the $(J-K)_0$ vs. K_0 CMD. These criteria were applied to the near-IR photometric catalogue of Sibbons et al. (2010) and the surface distribution of the C/M ratio was discussed. We used the C/M ratio as a metallicity indicator and found that the galaxy has an average metallicity index [Fe/H] $\sim -1.2 \div -1.3$ dex with a spread of Δ[Fe/H] $\sim 0.4 \div 0.6$ dex according to the different C/M vs. metallicity calibrations. Regions of larger C/M ratio (lower metallicity) are preferably distributed across a broken ellipse around the centre, which itself has a smaller ratio (higher metallicity). We also discussed whether the trends in the C/M ratio are driven by age rather than metallicity variations. A comparison with isochrones suggests that regions of higher C/M ratio are slightly older than the regions of lower C/M ratio.

The wide area of the IR catalogue allows us to investigate the field of NGC 6822 out to one degree from its centre. We detected a significant overdensity of possible AGB stars south-west of the galaxy centre, but confirmation of their membership would require spectroscopic data.

Acknowledgements. The spectroscopic observations were acquired together with L. Sibbons, whose assistance is gratefully acknowledged. We are indebted to Carlo Izzo for his dedicated support and development of the VIMOS pipeline, including comprehensive documentation and helpful suggestions on data reduction. We thank Antoniya Valcheva for useful comments and notes on the paper. We gratefully acknowledge funding for this project by the ESO DGDF grant. The project was partially funded by the Bulgarian NSF (contract No DDVU02/40/2010). This research has made use of the NASA/IPAC Extragalactic Database (NED) which is operated by the Jet Propulsion Laboratory, California Institute of Technology, under contract with the National Aeronautics and Space Administration. We thank the anonymous

referee and the editor Ralf Napiwotzki, whose comments helped to improve the paper.

References

Aaronson, M. & Mould, J. 1985, ApJ, 290, 191
Battinelli, P. & Demers, S. 2004, A&A, 416, 111
Battinelli, P. & Demers, S. 2005, A&A, 434, 657
Battinelli, P. & Demers, S. 2011, A&A, 525, 69
Battinelli, P., Demers, S., & Kunkel, W. E. 2006, A&A, 451, 99
Bertin, E. & Arnouts, S. 1996, A&AS, 117, 393
Bessell, M. S. & Brett, J. M. 1988, PASP, 100, 1134
Cassisi, S., Castellani, V., Degl'Innocenti, S., Piotto, G., & Salaris, M. 2001, A&A, 366, 578
Chandar, R., Bianchi, L., & Ford, H. C. 2000, AJ, 120, 3088
Cioni, M.-R. L. 2009, A&A, 506, 1137
Cioni, M.-R. L. & Habing, H. J. 2003, A&A, 402, 133
Cioni, M.-R. L. & Habing, H. J. 2005, A&A, 429, 837
Cioni, M.-R. L., Irwin, M., Ferguson, A. M. N., et al. 2008, A&A, 487, 131
Cioni, M.-R. L., Irwin, M., Ferguson, A. M. N., et al. 2009, A&A, 500, 1025
Clementini, G., Held, E. V., Baldacci, L., & Rizzi, L. 2003, ApJ, 588, 85
Davidge, T. J. 2003, PASP, 115, 635
Demers, S., Battinelli, P., & Artigau, E. 2006a, A&A, 456, 905
Demers, S., Battinelli, P., & Kunkel, W. 2006b, ApJ, 636, 85
Efremova, B. V.and Bianchi, L., Thilker, D. A., Neill, J. D., et al. 2011, ApJ, 730, 88
Feast, M. W., Abedigamba, O. P., & Whitelock, P. A. 2010, MNRAS, 408, 76
Gallart, C., Aparicio, A., Bertelli, G., & Chiosi, C. 1996, AJ, 112, 1950
Gallart, C., Aparicio, A., & Vilchez, J. M. 1996, AJ, 112, 1928
Gallart, C., Zoccali, M., & Aparicio, A. 2005, ARA&A, 43, 387
Girardi, L. & Marigo, P. 2007, A&A, 462, 237
Girardi, L., Williams, B. F., Gilbert, K. M., et al. 2010, ApJ, 724, 1030
Gorski, M., Pietrzynski, G., & Gieren, W. 2011, AJ, 141, 194
Gouliermis, D. A., Schmeja, S., Klessen, R. S., de Blok, W. J. G., & Walter, F. 2010, ApJ, 725, 1717
Groenewegen, M. A. T. 2004, arXiv:astro-ph/0407282, invited review at the conference: "Planetary Nebulae beyond the Milky Way"
Groenewegen, M. A. T., Lançon, A., & Marescaux, M. 2009, A&A, 504, 1031
Gullieuszik, M., Held, E. V., Rizzi, L., Girardi, L., & Marigo, P.and Momany, Y. 2008, MNRAS, 388, 1185
Hammersley, P., Christensen, L., Dekker, H., et al. 2010, The Messenger, 142, 8
Horne, K. 1986, PASP, 98, 609
Hutchings, J. B., Cavanagh, B., & Bianchi, L. 1999, PASP, 111, 559
Iben, I., J. & Renzini, A. 1983, ARA&A, 21, 271
Jacoby, G. H., Hunter, D. A., & Christian, C. A. 1984, ApJS, 56, 257
Karampelas, A., Dapergolas, A., Kontizas, E., & et al., L. 2009, A&A, 497, 703
Koribalski, B. S., Staveley-Smith, L., Kilborn, V. A., et al. 2004, AJ, 128, 16
Lançon, A. & Wood, P. R. 2000, A&A, 146, 217
Le Fèvre, O., Saisse, M., Mancini, D., et al. 2003, in Presented at the Society of Photo-Optical Instrumentation Engineers (SPIE) Conference, Vol. 4841, Society of Photo-Optical Instrumentation Engineers (SPIE) Conference Series, ed. M. Iye & A. F. M. Moorwood, 1670–1681
Lejeune, T., Cuisinier, F., & Buser, R. 1997, A&AS, 125, 229
Letarte, B., Demrs, S., Battinelli, P., & Kunkel, W. E. 2002, AJ, 123, 832
Lyubenova, M., Kuntschner, H., Rejkuba, M., et al. 2010, A&A, 510, A19+
Maraston, C. 2005, MNRAS, 362, 799
Maraston, C., Daddi, E., Renzini, A., et al. 2006, ApJ, 652, 85
Marigo, P. & Girardi, L. 2007, A&A, 469, 239
Marigo, P., Girardi, L., Bressan, A., et al. 2008, A&A, 482, 883
Mateo, M. L. 1998, ARA&A, 36, 435
Otto, E., Green, P. J., & Gray, R. O. 2011, ApJS, 196, 5
Robin, A. C., Reylé, C., Derrière, S., & Picaud, S. 2003, A&A, 409, 523
Scalo, G. M. & Miller, G. E. 1981, AJ, 248, 65
Schlegel, D. J., Finkbeiner, D. P., & Davis, M. 1998, ApJ, 500, 525
Sibbons, L. F., Cioni, M.-R. L., Irwin, M., & Rejkuba, M. 2010, ArXiv:1011.4464
Soubiran, C., Le Campion, J.-F., Cayrel de Strobel, G., & Caillo, A. 2010, A&A, 515, 111
Tolstoy, E., Irwin, M. J., Cole, A. A., et al. 2001, MNRAS, 327, 918
Turnshek, D. E., Turnshek, D. A., Craine, E. R., & Boeshaar, P. C. 1985, An atlas of digital spectra of cool stars (Tucson, Arizona 85745: Western Research Company)
Venn, K. A., Lennon, D. J., Kaufer, A., et al. 2001, ApJ, 547, 765
Ventura, P. & Marigo, P. 2010, MNRAS, 408, 2476
Weldrake, D. T. F., de Block, W. J. G., & Walter, F. 2003, MNRAS, 340, 12
Zacharias, N., Monet, D. G., Levine, S. E., et al. 2005, SIMBAD, 1297

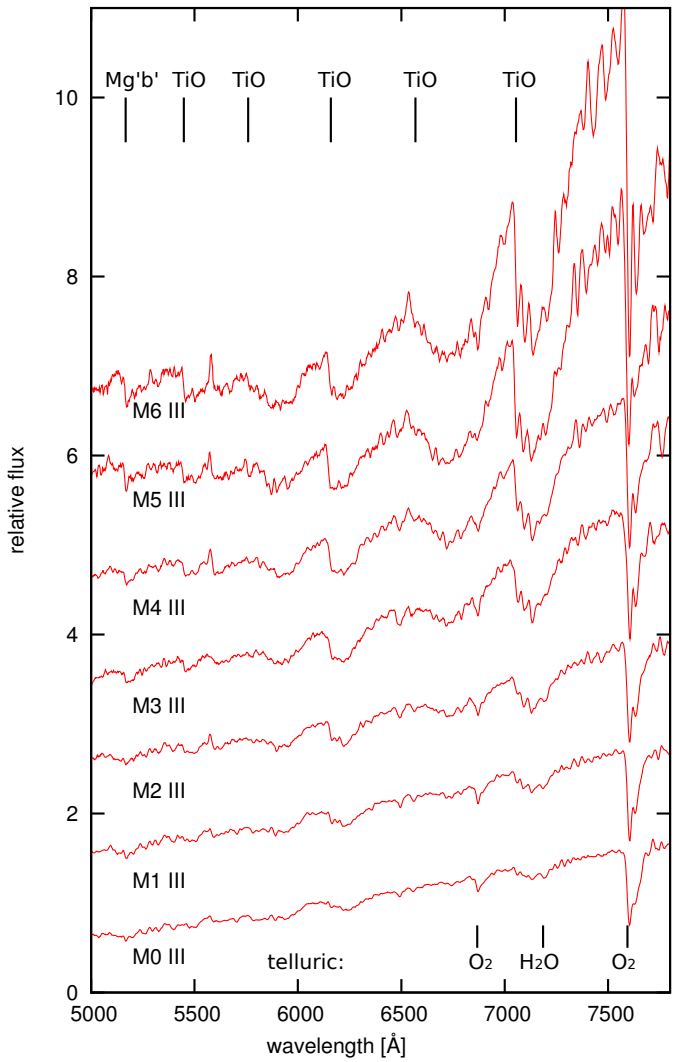

Fig. A.1. Full sample of average spectra for different spectral types giants according to our classification. The blue edge positions of some of the strongest TiO bands are shown with black lines as well as some telluric bands. The spectra are shifted along the y-axis with an arbitrary constant for presentation purposes.

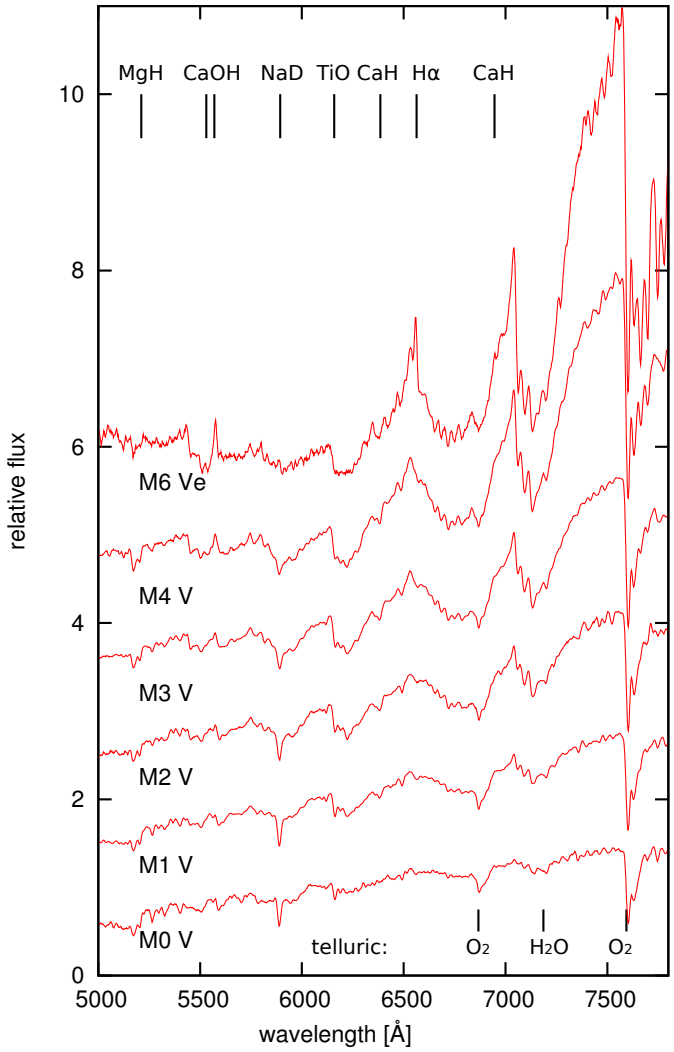

Fig. A.2. Full sample of average spectra for different spectral types dwarfs according to our classification. The positions of some of the most characteristic features as well as some telluric bands are shown with black lines. Among these are the sodium doublet (not resolved), the MgH, and the CaH bands. The spectra are shifted along the y-axis with an arbitrary constant for presentation purposes.

Appendix A: Full sample of M-type average spectra for giant and dwarf stars

Appendix B: Full spectrophotometric catalogue

Table B.1. Full spectrophotometric catalogue.

ID	X [px]	Y [px]	RA [deg]	DEC [deg]	r [deg]	R [mag]	J [mag]	H [mag]	K [mag]	Sp. Cl. photometry	Sp. Cl. spectroscopy	Quality flag
94208	219.732	1679.789	296.349976	−14.828187	0.1121527	19.772	17.877	17.0450	16.898	M	M1III	4
94979	330.734	1801.989	296.357117	−14.834526	0.1206048	19.509	17.528	16.7200	16.515	Mca	M1III	4
96968	608.073	1462.465	296.337067	−14.850516	0.1073543	18.978	16.924	16.0800	15.693	C	C5.5	5
97590	696.476	1751.644	296.354126	−14.855531	0.1249199	19.406	17.334	16.5210	16.218	M	C5.5	5
98478	830.038	930.973	296.306183	−14.863027	0.08862444	23.062	17.451	16.2840	15.489	C	–	4
99641	1001.033	2013.256	296.369537	−14.872893	0.1464667	20.196	17.025	15.9710	15.317	C	C6.5	5
100035	1068.920	652.043	296.289734	−14.876258	0.08785845	17.078	17.404	16.5370	15.991	C	–	4
101911	1355.722	158.286	296.260742	−14.892557	0.09137722	20.645	17.952	17.1530	16.985	M	M	4
77311	48.431	1099.388	296.316101	−14.679276	0.1453135	19.438	17.443	16.6010	16.179	C	C6.5	5
79509	475.349	2029.313	296.371155	−14.703938	0.1641518	20.219	18.079	17.1980	16.991	M	M1III	5
83906	1226.993	1566.500	296.343781	−14.746560	0.1178242	21.667	17.437	16.5320	16.128	C	C5.5	5
85530	1462.654	1902.611	296.363739	−14.759742	0.1306686	23.344	16.528	15.5650	14.986	C	C5.5	5
85885	1506.260	2089.456	296.374664	−14.762603	0.1401522	22.981	17.504	16.5860	16.355	M	M4III	5
88539	1880.543	1058.628	296.313934	−14.783896	0.07590062	22.971	17.388	16.3590	15.668	C	C5.5	4
77230	140.325	1975.243	296.193542	−14.678253	0.1337262	20.206	17.488	16.4980	16.071	C	C5.5	5
78095	311.616	1734.144	296.179352	−14.688039	0.1306334	19.813	17.241	16.3500	16.076	M	C5.5	5
78871	459.932	2256.131	296.210236	−14.696464	0.1111891	21.556	16.949	16.3370	15.919	M	dM5 e	5
79224	532.454	1875.599	296.187653	−14.700607	0.1156495	21.826	17.792	17.0730	16.777	M	M6.5III	5
79511	589.745	1521.752	296.166718	−14.703956	0.1239035	20.233	17.724	16.8900	16.697	M	M1III	4
80764	832.120	1828.010	296.184784	−14.717754	0.1022478	20.280	17.435	16.4590	16.039	C	C5.5	5
81015	879.108	1219.159	296.148743	−14.720551	0.1237123	20.331	18.060	17.2540	17.066	M	M1III	5
81290	923.831	1041.148	296.138214	−14.723130	0.130111	20.327	17.227	16.1880	15.542	C	C6.5	5
82246	1076.064	1643.366	296.173828	−14.731837	0.09789109	20.061	17.335	16.5430	16.299	M	M4III	6
83467	1267.180	2155.227	296.204193	−14.742633	0.07085879	18.691	15.048	14.1730	13.874	M	M6III	6
83752	1310.298	1599.732	296.171265	−14.745203	0.09053338	20.500	18.020	17.2280	16.970	M	C5.5	5
84020	1354.477	1830.278	296.185242	−14.747572	0.07863506	23.015	17.622	16.7990	16.588	M	dM	5
85975	1628.458	2046.414	296.197662	−14.763362	0.0587216	20.414	17.175	16.2550	15.536	C	C5.5	5
86798	1753.719	2238.658	296.208893	−14.769947	0.04610623	24.466	17.025	16.2010	15.758	C	C6.5	5
88152	1934.647	2076.698	296.199615	−14.780900	0.04676038	20.389	18.414	17.4210	17.201	C	M2III	5
88716	2021.618	2204.011	296.206879	−14.785284	0.03828439	19.733	18.082	17.2090	17.074	M	C5.5	5
93532	99.508	1716.032	296.178833	−14.822721	0.06469996	20.139	17.330	16.4750	16.210	M	SIII	5
93858	143.567	1738.309	296.180084	−14.825297	0.0643363	19.755	17.231	16.3660	15.897	C	C5.5	6
94446	230.224	2278.535	296.212219	−14.830112	0.03894694	20.872	17.270	16.3430	16.036	Cca	C8.2	5
94947	300.292	1631.935	296.173828	−14.834276	0.07354362	20.655	18.015	17.1510	16.987	Mca	M1III	5
95293	347.628	1413.000	296.160797	−14.836968	0.08655488	20.626	18.027	17.3700	17.092	Mca	dM3	6
95728	403.469	2278.123	296.212219	−14.840272	0.04650028	20.195	17.982	17.2200	16.969	Mca	M1III	5
96027	446.237	1980.717	296.194489	−14.842676	0.06054405	20.110	17.014	16.1110	15.568	C	C5.5	6
96655	534.901	2107.292	296.202057	−14.847754	0.05873197	20.336	17.178	16.1740	15.577	Cca	C5.5	6
97310	630.525	1483.251	296.164886	−14.853178	0.09058697	20.933	17.217	16.0280	15.151	C	C5.5 e	5
97913	716.647	1730.092	296.179565	−14.858191	0.08199306	20.623	17.341	16.3750	15.818	C	C5.5	6
98241	766.439	1879.345	296.188385	−14.861088	0.0777808	20.347	17.551	16.5470	16.182	C	C5.5	6
98573	817.915	1354.279	296.157288	−14.863935	0.1029569	20.610	17.318	16.4730	16.265	M	S4III	5
99143	899.102	1716.438	296.178772	−14.868636	0.08985176	20.434	17.478	16.4020	15.788	C	C5.5	5
99429	941.077	2155.420	296.204865	−14.871100	0.07652162	19.485	16.935	16.1020	15.807	M	C3.2	4
99831	1001.368	2176.731	296.206085	−14.874577	0.07907305	20.500	18.145	17.3370	17.039	M	M1III	5
100207	1059.988	1544.010	296.168549	−14.877820	0.103556	20.499	17.222	16.1570	15.564	C	C5.5	6
100545	1120.211	656.699	296.116089	−14.881053	0.146717	20.608	17.310	16.2500	15.450	C	C5.5	6
100929	1170.884	1554.526	296.169189	−14.884176	0.1077872	18.537	15.852	15.0160	14.782	M	M3III	6
101207	1213.494	1965.984	296.193604	−14.886700	0.09561194	20.821	18.299	17.3730	17.215	M	M1III	4
101866	1317.354	261.889	296.092773	−14.892178	0.1724127	20.724	17.214	16.1570	15.608	C	C6.5	5
102365	1382.647	2199.900	296.207458	−14.896397	0.09869482	20.202	17.393	16.5830	16.197	C	C5.5	5
102622	1429.550	698.842	296.118591	−14.898730	0.1548093	19.469	16.894	16.0340	15.732	M	C5.5	6
102922	1469.457	1946.731	296.192444	−14.901339	0.1091068	19.995	17.672	16.7560	16.644	M	M1III	5
103170	1512.781	637.136	296.114899	−14.903462	0.1606384	21.228	18.059	17.3320	17.124	M	dM	5
103686	1589.714	1849.405	296.186646	−14.908154	0.1178013	20.290	17.764	16.8700	16.708	M	M2III	5
105632	1911.998	2186.210	296.206696	−14.926620	0.1277681	20.623	16.997	15.8610	15.147	C	C6.5 e	5
106121	1995.065	1133.199	296.144318	−14.931097	0.1598977	20.290	17.520	16.6130	16.411	M	S4III	5
93464	115.145	1545.581	296.342345	−14.822172	0.1034667	19.982	17.481	16.5810	16.401	M	M3III	6
93781	159.119	1367.898	296.331849	−14.824688	0.09370232	19.914	18.029	17.0300	16.852	M	M1III	5
94073	198.307	1365.637	296.331716	−14.826927	0.09410673	19.681	17.657	16.8000	16.693	M	M0III	4
94429	251.999	1710.987	296.351776	−14.830035	0.1143249	19.629	17.677	16.9310	16.712	Mca	C8.2	5
94986	330.474	1607.357	296.345673	−14.834577	0.109602	19.646	17.219	16.3410	15.898	Cca	C5.5	5
95355	381.519	188.258	296.262573	−14.837487	0.04053589	21.772	17.440	16.6190	16.297	Mca	–	4
96598	552.443	1569.942	296.343445	−14.847301	0.1118206	19.728	17.905	17.0470	16.885	Mca	M0III	5
97225	643.947	1948.517	296.365814	−14.852487	0.1344904	19.955	17.293	16.2590	15.570	C	C5.5	6
97567	692.912	1625.477	296.346741	−14.855356	0.118171	19.721	17.320	16.4810	16.022	C	C5.5	6
100023	1057.845	2118.620	296.375763	−14.876107	0.1534723	20.461	17.948	17.0280	16.819	M	M4III	6
100521	1140.994	1899.504	296.363129	−14.880856	0.1449505	20.763	17.439	16.5950	16.435	M	M	4
101802	1328.222	1947.256	296.365631	−14.891643	0.1530257	17.818	15.562	14.7120	14.318	C	M5III	6
102163	1381.521	181.820	296.261505	−14.894732	0.09366731	19.226	17.792	16.8330	16.802	M	M	4
103115	1528.656	1432.273	296.335785	−14.902986	0.1377446	22.048	17.233	16.4110	16.022	C	M	4
104988	1839.747	603.009	296.286987	−14.920337	0.1257777	20.379	16.908	16.0870	15.896	M	M4III	6
105583	1936.177	395.957	296.275116	−14.926181	0.1275145	17.681	18.321	17.4000	17.123	C	M	4
100901	1194.765	2204.951	296.380829	−14.883905	0.1616888	19.816	17.628	16.7630	16.596	M	M2III	6
77470	79.012	1424.934	296.335388	−14.681108	0.1547554	20.811	18.391	17.5060	17.091	C	C6.5	5
78605	300.450	1175.215	296.320587	−14.693704	0.1357911	20.496	18.135	17.2270	17.169	M	M4III	5
79960	565.862	723.431	296.293854	−14.708783	0.1086049	19.802	17.537	16.5730	16.344	C	C8.2	5
80354	632.794	1973.000	296.367828	−14.712914	0.1561492	19.776	17.585	16.7650	16.497	M	M1III	5
81804	893.125	2201.301	296.381348	−14.727878	0.1597525	19.818	17.516	16.6270	16.418	M	M4III	6
82163	951.905	1764.820	296.355621	−14.731111	0.1358754	20.880	18.112	17.4290	17.172	M	dM	4
83580	1183.490	576.054	296.285706	−14.743645	0.07489761	19.592	17.682	16.8610	16.682	M	M2III	6
86652	1624.801	181.656	296.262848	−14.768750	0.04120793	20.685	17.647	16.7960	16.637	M	C6.5	5
88480	1876.425	807.580	296.299103	−14.783449	0.06183038	21.817	17.480	16.5290	15.729	C	C	4
77118	113.750	977.699	296.134644	−14.676920	0.1650128	20.201	17.350	16.3210	15.771	C	C5.5	5

ID	X [px]	Y [px]	RA [deg]	DEC [deg]	r [deg]	R [mag]	J [mag]	H [mag]	K [mag]	Sp. Cl. photometry	Sp. Cl. spectroscopy	Quality flag
77316	154.446	752.842	296.121368	−14.679315	0.1720997	19.923	17.359	16.3990	16.029	C	C5.5	5
77799	256.279	1720.472	296.178497	−14.684889	0.1338186	20.476	18.044	17.0830	16.866	M	M	4
78016	295.369	1565.082	296.169312	−14.687134	0.136401	20.830	17.699	17.0310	16.750	M	dM	5
78454	380.001	1322.182	296.154877	−14.691996	0.1405851	21.633	17.839	17.2650	16.853	M	dM6	5
78876	459.092	1578.631	296.170105	−14.696488	0.1280806	20.142	17.366	16.4390	16.089	C	C5.5	5
79197	526.400	2131.135	296.202850	−14.700215	0.109898	20.626	17.115	15.9860	15.382	C	C6.5	5
79433	571.227	1337.355	296.155792	−14.702925	0.1314986	20.337	17.811	17.1140	16.901	M	dM3.5	5
79980	675.042	971.264	296.134155	−14.708930	0.1423327	20.065	17.268	16.4270	16.191	M	M	4
80222	723.850	1745.948	296.179932	−14.711598	0.1100565	20.488	18.122	17.2810	17.030	M	M	4
80491	772.563	606.993	296.112671	−14.714574	0.1557517	18.860	16.424	15.5170	15.338	M	M0III	5
80754	828.488	1871.651	296.187347	−14.717557	0.1010392	20.633	17.671	16.7230	16.491	C	–	4
80959	869.466	2050.729	296.198029	−14.719869	0.09377533	20.698	17.606	16.4790	15.802	C	C6.5	5
81277	922.290	442.212	296.103516	−14.723016	0.1589202	21.351	17.447	16.5450	16.070	C	–	4
81701	991.628	1257.945	296.151001	−14.726998	0.1177624	19.754	16.872	16.0000	15.486	C	C5.5	5
82019	1039.928	864.474	296.127747	−14.729833	0.1347219	20.382	17.725	16.9170	16.640	M	M0III	4
82395	1106.941	1397.912	296.159454	−14.733295	0.107247	21.045	17.518	16.5720	15.920	C	C6.5	5
82849	1168.330	1736.295	296.179535	−14.737016	0.09021352	20.854	17.065	16.0540	15.353	C	–	4
83463	1265.682	1736.553	296.179321	−14.742605	0.08633379	19.952	17.415	16.4900	15.870	C	C6.5	5
83731	1309.487	2204.519	296.207184	−14.745038	0.06727213	20.060	17.006	15.9930	15.379	C	C5.5	5
84687	1445.366	1738.338	296.179443	−14.752915	0.07931381	19.452	16.663	15.7340	15.234	C	C5.5	5
84957	1487.245	2148.610	296.203827	−14.755259	0.06059641	20.677	17.967	17.1640	16.598	C	C6.5	5
85283	1529.437	1775.746	296.181671	−14.757700	0.07458314	19.873	17.175	16.2820	15.944	C	C6.5	5
87260	1809.503	2128.361	296.202637	−14.773767	0.04816949	20.774	17.296	16.4140	15.714	C	C	4
87885	1898.351	1850.164	296.186096	−14.778706	0.05984022	20.502	16.722	15.9020	15.543	M	C6.5	5
88232	1946.670	1974.430	296.193481	−14.781586	0.05192688	20.129	17.935	17.1620	16.883	M	M0III	4
93440	85.371	1976.149	296.194275	−14.821965	0.04988627	19.925	17.296	16.4080	15.902	C	C5.5	5
93738	128.424	1795.840	296.183502	−14.824387	0.06081326	20.045	17.580	16.7570	16.576	M	M0III	4
94114	181.327	1459.939	296.163879	−14.827393	0.0803668	21.628	17.105	15.9910	15.211	C	–	5
94394	221.827	1776.910	296.182404	−14.829756	0.06386462	19.725	17.808	16.9830	16.854	Mca	M0III	4
94807	281.343	1490.337	296.165405	−14.833178	0.08085636	20.082	17.271	16.4480	16.238	Mca	S	4
95088	322.905	1150.017	296.145233	−14.835481	0.1005995	19.797	18.002	17.1820	17.032	Mca	M	4
95439	368.630	980.065	296.135132	−14.838089	0.1110075	19.925	17.570	16.6770	16.486	Mca	M2III	5
95858	421.958	1951.231	296.192749	−14.841306	0.06101953	20.344	18.047	17.3000	17.066	Mca	M0III	5
96249	479.884	1570.421	296.170105	−14.844587	0.08162148	21.037	17.354	16.2340	15.509	Cca	C6.5	6
97298	626.818	1863.475	296.187469	−14.853082	0.07271314	20.402	18.169	17.2890	17.198	M	M0III	5
97868	708.577	1933.343	296.191681	−14.857764	0.07310484	20.214	17.902	16.9560	16.761	M	M0III	5
98231	766.912	1335.598	296.156158	−14.860965	0.1021718	20.326	17.108	16.2140	15.634	C	C6.5	5
98508	806.540	1863.038	296.187439	−14.863374	0.08011466	20.740	18.029	17.0310	16.932	M	M0III	4
98786	848.109	1598.377	296.171783	−14.865685	0.09279083	19.938	17.105	16.1450	15.625	C	C6.5	5
99102	896.777	602.254	296.112885	−14.868258	0.1432176	20.504	17.170	16.1960	15.588	C	C6.5	6
99420	941.606	1597.766	296.171753	−14.870989	0.09645104	20.524	18.017	17.2690	17.046	M	M0III	5
99756	991.908	1883.876	296.188690	−14.873989	0.08759131	20.788	17.872	16.9830	16.879	M	M2III	5
100040	1032.732	1714.890	296.178711	−14.876316	0.09561086	20.439	18.070	17.0830	16.720	C	C5.5	5
100308	1075.191	1323.477	296.155457	−14.878673	0.1136186	20.832	17.625	16.4290	15.762	C	C6.5	6
100873	1160.316	2034.451	296.197540	−14.883656	0.09104712	20.752	17.866	16.7780	16.200	C	C6.5	5
101165	1206.733	2101.514	296.201691	−14.886331	0.09157387	19.856	16.685	15.6190	15.007	C	C6.5	6
102136	1351.697	1452.545	296.163086	−14.894490	0.1195779	19.627	16.753	15.8810	15.436	C	C6.5	5
102372	1390.186	686.085	296.117828	−14.896477	0.15404	20.419	17.798	16.9680	16.867	M	M2III	5
102696	1434.310	2033.187	296.197540	−14.899305	0.1050971	19.457	17.107	16.2950	16.098	M	M1III	6
102923	1476.325	644.635	296.115417	−14.901344	0.1589198	20.026	17.706	16.9500	16.771	M	M0III	4
103386	1549.772	211.411	296.089813	−14.905375	0.1820071	20.747	17.896	16.8550	16.316	C	C6.5	5
105264	1848.100	1614.061	296.172760	−14.922873	0.1373595	19.289	16.532	15.6700	15.261	C	C5.5	6
105623	1912.787	1678.954	296.176575	−14.926566	0.1387822	20.516	18.216	17.4150	17.113	M	M0III	4
105963	1966.918	1630.843	296.173828	−14.929623	0.1427653	20.596	17.362	16.4860	16.301	M	M	4
91631	2023.499	2238.914	296.233276	−14.808039	0.008645295	19.292	17.538	16.6880	16.465	M	C	5
66772	271.986	1836.046	296.209412	−14.569217	0.2362787	21.103	17.453	16.3900	15.660	C	C	4
68853	641.390	2227.626	296.232605	−14.590483	0.2130963	20.271	17.931	17.3520	17.046	M	dM2	5
69102	687.032	1852.373	296.210419	−14.592963	0.2126182	22.248	17.963	17.3480	17.033	M	dM6 e	5
69707	799.382	1765.816	296.205383	−14.599363	0.2070814	19.85	17.083	16.5110	16.279	M	dM3	5
70265	895.744	1822.741	296.208740	−14.604931	0.2010376	19.974	18.102	17.3850	17.319	M	dM1.5	5
70561	952.491	1516.451	296.190643	−14.608078	0.2016357	19.700	17.586	16.7320	16.563	M	M1III	4
71373	1083.118	1955.730	296.216583	−14.615705	0.1892534	19.679	17.813	17.2010	16.998	M	dM1.5	5
71915	1178.857	1911.945	296.214020	−14.621172	0.1841841	19.406	17.390	16.7630	16.607	M	dM1.5	5
73986	1563.103	1499.868	296.189636	−14.643152	0.1681821	20.018	17.088	16.4810	16.215	M	dM3	5
74248	1610.372	2242.038	296.233551	−14.646070	0.157517	20.175	17.741	17.0570	16.927	M	dM3	5
74874	1722.664	2169.424	296.229279	−14.652489	0.1513638	21.271	17.698	16.4220	15.496	C	C8.2	5
76015	1938.009	1570.511	296.193878	−14.664783	0.1463041	20.917	18.340	17.6050	17.257	M	C8.2 e	5
64758	36.428	1591.632	296.020721	−14.549389	0.3359747	21.499	18.370	17.6100	17.368	M	M4III	5
65037	78.187	884.627	295.978973	−14.551923	0.3629036	19.744	17.750	16.9830	16.768	M	M1III	5
66587	352.643	2243.055	296.059235	−14.567330	0.2977124	20.174	17.994	17.2600	17.157	M	dM1	4
67210	462.207	1187.923	295.996796	−14.573745	0.3349485	19.985	18.158	17.3490	17.201	M	M1III	5
67490	502.352	919.435	295.981812	−14.576805	0.3439837	20.922	17.368	16.7900	16.532	M	–	4
68054	614.424	927.944	295.981445	−14.582492	0.340543	19.965	18.026	17.3390	17.126	M	dM0	4
68809	744.393	343.917	295.946991	−14.590075	0.3629333	21.382	18.303	17.8080	17.445	M	dM4.5	4
69935	932.110	933.213	295.982422	−14.601364	0.3278433	20.898	17.967	17.2110	16.981	M	dM	4
70482	1051.859	1927.081	296.040436	−14.607334	0.2802055	20.792	18.163	17.0850	16.646	C	C5.5	5
70854	1111.583	2023.260	296.046143	−14.610744	0.2737469	20.522	17.597	16.9440	16.602	M	dM	4
71314	1190.897	2148.824	296.053589	−14.615259	0.2652877	20.918	17.901	17.1440	16.860	M	dM	5
71622	1242.060	2048.220	296.047607	−14.618206	0.2674887	20.069	18.222	17.5730	17.431	M	dM0	4
72115	1331.568	2083.472	296.049713	−14.623334	0.262428	19.518	17.918	17.2310	17.082	M	dM0	4
72930	1482.881	1652.719	296.024170	−14.632055	0.2760559	19.379	17.776	17.1480	16.904	M	dM0	6
73293	1550.059	1233.343	295.999390	−14.635953	0.2936424	20.416	17.817	16.8960	16.458	C	C5.5	5
74069	1689.607	1012.810	295.986328	−14.643986	0.300119	20.589	17.983	17.2240	16.969	M	dM3	5
74550	1784.638	1560.359	296.018707	−14.649366	0.2701253	19.133	17.628	16.9330	16.816	M	dM0	4
75067	1877.186	2207.495	296.057068	−14.654613	0.2362768	20.143	17.773	16.9260	16.688	M	M5III	5
75313	1923.682	1554.316	296.018372	−14.657308	0.2659556	20.211	17.694	17.0560	16.876	M	dM3.5	5

ID	X [px]	Y [px]	RA [deg]	DEC [deg]	r [deg]	R [mag]	J [mag]	H [mag]	K [mag]	Sp. Cl. photometry	Sp. Cl. spectroscopy	Quality flag
75540	1963.513	1703.963	296.027252	−14.659583	0.2573032	20.072	17.632	17.0850	16.740	M	dM3.5	4
75867	2024.368	1262.663	296.001099	−14.663127	0.2775622	19.762	17.754	17.0790	16.836	M	dM1.5	4
81688	570.837	2097.862	296.051239	−14.726850	0.2042504	20.360	17.414	16.3970	15.734	C	C6.5	5
83473	847.842	1881.308	296.038330	−14.742747	0.211167	20.770	17.513	17.0260	16.573	M	dM4	5
84913	1062.010	1524.746	296.017212	−14.754925	0.2285835	19.124	17.626	17.1190	16.727	M	dM0	5
85472	1135.475	2196.149	296.057068	−14.759219	0.1887721	21.963	17.951	17.3430	16.984	M	dM	5
86142	1229.374	2201.857	296.057373	−14.764623	0.1872817	19.872	18.174	17.4660	17.283	M	–	4
86680	1308.239	1484.110	296.014832	−14.769041	0.2283621	20.342	17.050	15.8860	15.051	C	C8.2	5
87702	1450.661	459.303	295.954315	−14.777233	0.2874711	23.446	18.212	17.5830	17.391	M	M	4
88306	1537.470	1958.039	296.042908	−14.782191	0.1988197	19.580	16.913	15.9700	15.401	C	C5.5	5
89403	1686.545	1670.320	296.025879	−14.790672	0.2150897	19.888	17.776	16.9470	16.628	M	M3III	5
90158	1794.297	1590.511	296.021149	−14.796692	0.2195444	20.412	17.356	16.2890	15.713	C	C5.5	5
90520	1840.639	1975.324	296.043915	−14.799509	0.1967141	20.082	17.434	16.7460	16.545	M	dM3.5	5
91028	1912.652	1588.543	296.021088	−14.803503	0.219502	18.917	17.093	16.4280	16.264	M	dM1.5	5
91442	1964.455	1520.768	296.017029	−14.806444	0.2235813	20.304	17.862	17.2390	17.061	M	dM3	5
80256	329.809	585.619	296.431030	−14.711975	0.2112613	19.278	17.788	17.0890	16.928	M	dM	4
80997	475.254	388.976	296.419373	−14.720345	0.1971457	20.442	17.697	17.0840	16.839	M	–	4
81226	516.494	1524.360	296.486694	−14.722583	0.2590432	19.929	17.480	16.8500	16.665	M	–	4
81582	571.134	892.854	296.449310	−14.725839	0.2226754	19.853	17.417	16.4770	16.316	M	M	4
82227	673.160	392.833	296.419983	−14.731664	0.1932153	23.406	17.538	16.6900	16.500	M	M0III	4
82894	773.197	840.505	296.276184	−14.737480	0.07494187	21.001	17.378	17.3270	16.362	M	–	4
83291	837.520	1496.135	296.484985	−14.741018	0.2522382	20.868	17.769	17.2150	16.860	M	–	4
83620	898.489	272.818	296.412872	−14.743980	0.1822508	21.161	18.142	17.5280	17.187	M	–	4
84497	1021.553	2126.345	296.522186	−14.751385	0.2863651	19.041	16.181	15.5830	15.298	M	dM4	5
84810	1061.870	512.649	296.426727	−14.754023	0.1925824	19.853	17.422	16.4230	15.825	C	C6.5	5
85162	1113.206	1505.228	296.485504	−14.756813	0.249311	18.674	16.735	15.9320	15.627	M	C8.2	5
85886	1212.079	779.046	296.442505	−14.762609	0.206	20.355	17.138	15.9980	15.096	C	C6.5	5
86205	1260.901	1741.136	296.499451	−14.765201	0.2616686	23.605	18.201	17.5790	17.225	M	–M	4
86700	1334.883	627.695	296.433807	−14.769137	0.1962366	23.668	17.658	17.0300	16.882	M	dM3	5
87313	1422.183	197.216	296.408356	−14.774137	0.1703041	19.583	18.124	17.4070	17.179	M	M	4
89698	1746.850	1906.374	296.509125	−14.792881	0.2687421	20.160	16.943	16.3310	16.043	M	dM	5
90095	1807.192	783.773	296.442902	−14.796197	0.2024412	23.183	17.512	16.6470	16.456	M	M2III	5
90841	1903.101	1427.997	296.480835	−14.801933	0.2402497	19.534	17.491	16.6740	16.423	M	C6.5	5
91572	2000.393	1153.676	296.464600	−14.807542	0.2240478	20.002	17.144	16.2310	15.567	C	–	4
65740	83.494	1324.174	296.475342	−14.558714	0.339108	20.101	17.332	16.7230	16.514	M	dM3	5
67206	342.189	1993.754	296.514954	−14.573689	0.3578496	20.874	17.496	16.9270	16.638	M	dM3.5	4
67628	419.191	1979.323	296.514130	−14.578083	0.3544083	20.025	18.111	17.5010	17.224	M	dM1.5	5
68304	537.417	1929.632	296.511230	−14.584842	0.3478887	20.770	17.755	16.7900	16.308	C	C6.5	5
68961	659.290	733.064	296.440369	−14.591502	0.2912472	19.693	16.866	16.3160	16.045	M	dM3	5
69615	779.582	625.081	296.433899	−14.598368	0.2818131	19.476	17.976	17.2270	17.130	M	dM0	5
69875	818.666	1443.067	296.482483	−14.600801	0.3155481	19.328	17.206	16.5400	16.322	M	dM3	5
70172	872.047	1530.197	296.487640	−14.603875	0.3175779	18.773	17.107	16.4960	16.297	M	dM0	5
70629	952.486	1864.062	296.507385	−14.608586	0.3303689	21.680	17.734	17.0810	16.813	M	dM	5
70946	1014.252	433.919	296.422607	−14.611832	0.2642723	20.152	17.413	16.8020	16.563	M	dM3.5	5
71229	1054.676	2097.428	296.521149	−14.614511	0.338236	20.662	18.270	17.2260	16.797	C	C6.5	5
71613	1123.286	510.242	296.427124	−14.618094	0.2629529	20.598	17.826	17.2940	17.072	M	dM4.5	4
71939	1175.463	2092.198	296.520874	−14.621428	0.3341911	21.007	17.435	16.7900	16.587	M	dM	5
72429	1265.843	1825.571	296.505188	−14.626554	0.318272	19.421	17.942	17.3540	17.140	M	dM0	5
72667	1313.023	1884.647	296.508667	−14.629275	0.3196797	19.134	17.350	16.7620	16.565	M	dM0	5
72881	1357.042	699.647	296.438385	−14.631576	0.2620239	19.561	17.726	17.1120	16.907	M	dM1.5	5
73147	1404.084	1568.902	296.489960	−14.634430	0.3012412	20.002	18.087	17.3670	17.147	M	M0.5III	4
73508	1469.541	1550.219	296.488861	−14.638191	0.2982319	20.405	17.496	16.5570	15.974	C	C6.5 v	5
73972	1552.138	1714.834	296.498657	−14.642962	0.3038888	18.995	17.604	16.9870	16.826	M	dM0	4
75055	1762.340	1546.595	296.488434	−14.654464	0.2891667	22.259	18.159	17.4900	17.160	M	M0.5III	5
65002	68.477	1499.508	296.311554	−14.551598	0.2616391	20.918	17.914	17.3560	16.982	M	dM	5
65342	127.319	1760.287	296.326904	−14.554912	0.26308	19.651	17.650	17.0640	16.825	M	dM 1.5	4
65766	195.633	765.615	296.268188	−14.559031	0.2459519	20.383	18.014	17.4030	17.212	M	dM	4
66012	242.114	2158.067	296.350433	−14.561425	0.2657663	19.760	16.954	16.3720	16.114	M	dM3.5	5
66239	281.961	1299.193	296.299713	−14.563828	0.2467883	21.034	18.070	17.5170	17.256	M	dM	5
66625	349.998	1214.854	296.294617	−14.567719	0.2418231	21.074	18.624	17.7570	17.118	C	–	4
66989	414.807	996.517	296.281769	−14.571457	0.2355992	19.706	17.124	16.5230	16.283	M	dM3	5
67256	463.195	785.627	296.269318	−14.574274	0.2309493	21.220	18.240	17.5910	17.344	M	dM	5
67591	522.149	454.445	296.249817	−14.577723	0.2258951	20.474	17.969	17.3390	17.188	M	dM3.5	5
67835	567.063	462.604	296.250244	−14.580280	0.2233583	20.659	18.098	17.5090	17.201	M	dM	5
68214	636.571	1798.562	296.329102	−14.584000	0.2366088	19.231	17.611	16.9570	16.665	M	MIII e v	4
69259	822.208	722.901	296.265533	−14.594790	0.2101253	20.017	17.966	17.1110	16.840	M	M0III	5
69502	868.376	1319.641	296.300781	−14.597308	0.2147302	19.963	17.733	17.0420	16.821	M	dM3	4
69952	942.311	1055.177	296.285156	−14.601586	0.206705	18.981	16.715	16.0350	15.832	M	dM3	5
70257	1001.317	1673.565	296.321686	−14.604838	0.2145115	18.477	16.639	15.9480	15.801	M	dM1.5	5
71083	1143.816	1541.152	296.313812	−14.613031	0.2039929	19.722	17.510	16.6550	16.449	M	M1III	5
71579	1226.105	1338.001	296.301788	−14.617753	0.1955019	21.206	17.604	17.0050	16.654	M	dM	5
71937	1287.981	891.731	296.275482	−14.621393	0.1853504	20.537	17.978	17.2840	17.082	M	dM	4
72546	1401.148	694.722	296.263794	−14.627904	0.1770527	21.046	17.956	17.3170	17.003	M	dM	4
72871	1463.207	466.148	296.250305	−14.631506	0.1721979	19.227	17.544	16.8610	16.712	M	dM0	5
73481	1576.007	740.405	296.266541	−14.637911	0.1675406	19.640	17.655	17.0020	16.850	M	dM0	4
73816	1639.284	1755.617	296.326508	−14.641376	0.183421	19.640	16.649	15.6970	15.114	C	C5.5	6
74372	1743.443	954.590	296.279144	−14.647496	0.1606291	20.201	17.865	16.9980	16.804	M	M0III	4
74650	1794.341	1598.383	296.317230	−14.650301	0.1712368	19.966	17.816	17.2410	17.037	M	dM1.5III	5
74939	1843.750	886.658	296.275116	−14.653234	0.1541128	19.697	17.484	16.6120	16.452	M	M0III	4
75203	1895.875	1892.482	296.334686	−14.656092	0.1748211	20.152	17.954	17.3530	17.134	M	dM1.5	4
75443	1937.531	1315.076	296.300446	−14.658543	0.1567637	19.852	17.553	16.8810	16.693	M	dM2	4
75858	2020.282	1564.547	296.315430	−14.663013	0.1591158	21.691	17.486	16.8450	16.571	M	M4III	4
79984	247.486	671.188	296.263336	−14.708953	0.09717618	20.958	17.071	16.0530	15.567	C	C	3
80566	368.177	704.340	296.264954	−14.715384	0.09135444	20.125	17.411	16.4350	16.041	C	C6.5	5
80813	421.050	243.961	296.237854	−14.718291	0.08518256	18.971	17.509	16.6930	16.529	M	M0III	4
81082	466.164	1813.561	296.330536	−14.721181	0.1218816	20.879	17.693	16.8300	16.557	M	M4III	6

ID	X [px]	Y [px]	RA [deg]	DEC [deg]	r [deg]	R [mag]	J [mag]	H [mag]	K [mag]	Sp. Cl. photometry	Sp. Cl. spectroscopy	Quality flag
81620	556.993	971.522	296.280762	−14.726241	0.08701649	19.971	18.015	17.1460	17.061	M	C6.5	5
81886	598.398	1497.908	296.311920	−14.728691	0.1033142	20.084	17.538	16.7200	15.967	C	C6.5	5
83058	777.786	1602.111	296.318024	−14.739033	0.1007122	19.599	17.173	16.3780	15.970	C	C5.5	5
83368	826.641	1023.032	296.283783	−14.741738	0.07530929	20.344	18.103	17.2460	16.869	C	C5.5	5
83737	882.398	1969.443	296.339813	−14.745103	0.1150965	19.951	18.044	16.8820	16.328	C	C6.5	5
84531	1001.444	891.879	296.276062	−14.751641	0.06277198	20.366	17.531	16.6420	16.026	C	C6.5	5
84882	1056.758	356.340	296.244446	−14.754674	0.04890785	19.349	17.250	16.4940	16.217	M	C5.5	5
85196	1096.573	485.641	296.252136	−14.757003	0.04784077	19.901	17.914	16.9780	16.427	C	C5.5	5
85520	1139.406	1031.201	296.284271	−14.759642	0.06184969	19.962	17.737	16.9920	16.736	M	M0III	4
85795	1182.164	541.893	296.255432	−14.761878	0.04412279	20.016	17.528	16.6650	16.460	M	M1III	5
86182	1236.025	430.305	296.248871	−14.764977	0.03933418	21.013	17.110	15.9940	15.228	C	C8.2	5
86531	1278.603	1805.144	296.330048	−14.767764	0.0963056	20.116	17.105	16.0800	15.383	C	C6.5	5
86770	1317.775	645.294	296.261536	−14.769683	0.03971861	19.877	17.345	16.4830	16.072	C	C5.5	5
87610	1434.983	799.438	296.270599	−14.776425	0.04037064	19.601	18.035	17.1780	17.109	M	M0III	4
87928	1477.470	1316.896	296.301117	−14.779015	0.06526554	19.885	17.097	16.1570	15.672	C	C6.5	5
88274	1525.591	2112.354	296.348297	−14.781917	0.1098344	20.509	17.876	16.9140	16.802	M	M2III	5
88593	1568.969	1415.873	296.307007	−14.784284	0.06912143	19.709	16.947	16.0620	15.609	C	C5.5	5
88820	1608.607	546.488	296.255737	−14.786252	0.022902	20.022	18.197	17.2900	17.169	M	M	4
89202	1655.444	1253.420	296.297485	−14.789169	0.05865497	19.802	17.918	17.0920	16.867	M	M2III	5
90313	1816.286	220.722	296.236420	−14.797890	0.006933694	21.360	17.253	16.5160	16.222	M	C6.5	5
90637	1856.493	647.940	296.261719	−14.800416	0.02134283	21.380	17.985	17.1260	16.916	M	M5III	4
91024	1913.444	320.859	296.242493	−14.803477	0.00190359	20.070	18.038	17.1220	16.902	M	M2III	5
91382	1957.015	256.646	296.238708	−14.806007	0.003191378	19.831	17.348	16.5990	16.247	M	C6.5	5
91707	1997.193	845.672	296.273346	−14.808517	0.03314871	20.713	17.578	16.7360	16.420	M	S	5
84083	935.350	2255.019	296.356781	−14.748176	0.1286597	19.650	17.254	16.3290	15.885	C	–	5
107819	152.578	2269.796	296.539215	−14.949409	0.3323957	20.557	18.030	17.4290	17.225	M	dM3 e	5
108073	197.796	1607.195	296.500092	−14.952188	0.299116	20.466	17.307	16.7160	16.356	M	dM4	5
108343	249.356	1132.747	296.471954	−14.955172	0.2766858	18.844	17.722	17.0680	16.933	M	dK7	5
108575	298.031	1953.133	296.520447	−14.957832	0.3196248	20.108	17.232	16.7060	16.401	M	dM3.5	6
108866	343.659	1497.908	296.493561	−14.960535	0.2977859	19.605	17.634	17.0230	16.841	M	dM1.5	6
109349	437.068	1437.840	296.490021	−14.965914	0.2976861	19.616	17.821	17.0120	16.765	M	M0III	4
109635	489.949	1234.866	296.478027	−14.968984	0.2894557	20.613	17.479	16.9030	16.598	M	dM4	5
110106	579.800	1255.259	296.479218	−14.974156	0.2934124	19.889	16.882	15.9430	15.387	C	C5.5	5
110336	627.393	2173.258	296.533447	−14.976672	0.3402619	19.406	17.957	17.2850	17.100	M	dM0	6
110613	675.433	1370.504	296.485962	−14.979607	0.3020694	19.307	17.895	17.2330	17.128	M	dM0	6
110981	748.585	1019.129	296.465210	−14.983861	0.2881139	19.862	17.958	17.1160	16.919	M	M0III	4
111332	816.107	1483.753	296.492737	−14.987658	0.3122791	20.114	18.286	17.5050	17.368	M	M0III	4
111564	858.497	1887.966	296.516693	−14.989991	0.3332237	20.227	17.773	17.1190	16.923	M	dM3.5	5
111944	934.033	2279.147	296.539673	−14.994203	0.3547466	20.465	17.858	17.2170	16.951	M	dM3.5	5
112310	999.252	666.899	296.444275	−14.998292	0.2818846	20.377	18.018	17.4180	17.160	M	dM3.5	5
112524	1044.221	2063.887	296.526947	−15.000549	0.3476441	20.041	16.933	16.3220	15.973	M	dM4.5	5
112808	1097.347	1807.877	296.511871	−15.003676	0.3371824	19.629	17.720	16.8860	16.675	M	M1III	5
113033	1138.436	2061.343	296.526825	−15.005964	0.3506432	19.500	17.634	16.9950	16.810	M	dM1.5	5
113320	1190.035	510.484	296.435181	−15.009061	0.2831076	21.331	17.991	17.1300	16.915	M	M0III	4
113562	1230.043	707.132	296.446594	−15.011467	0.292775	20.420	17.572	16.9740	16.786	M	dM4.5	5
113871	1296.557	1952.948	296.520386	−15.015034	0.3508022	20.536	18.105	17.4920	17.135	M	dM3.5	5
114094	1339.564	2159.184	296.532562	−15.017410	0.3619879	20.634	17.862	17.3580	17.106	M	dM4.5	4
114787	1474.073	1868.528	296.515411	−15.025197	0.3531393	18.912	17.469	16.7880	16.638	M	dM0	6
115327	1579.255	1302.058	296.481842	−15.031350	0.3318889	19.575	17.875	17.1340	16.951	M	M0III	4
115580	1629.493	808.976	296.452637	−15.034349	0.3135087	19.658	17.328	16.7200	16.514	M	dM3	5
116285	1764.125	1573.307	296.497864	−15.041821	0.3507426	19.851	17.980	17.4040	17.235	M	dM1.5	5
116546	1813.885	2096.641	296.528717	−15.044480	0.3756627	19.881	17.686	17.1200	16.767	M	dM3	5
116777	1856.820	1534.154	296.495544	−15.047131	0.3526924	20.987	16.981	16.5000	16.109	M	dM6 e	5
117100	1924.159	1310.010	296.482300	−15.051053	0.3460362	19.661	17.559	16.8980	16.763	M	dM2	5
117329	1977.229	1558.586	296.496918	−15.053953	0.3584216	20.434	17.657	17.0260	16.701	M	dM	5
91077	40.182	957.984	296.462097	−14.803963	0.2215076	20.333	17.895	17.0680	16.914	M	M4III	6
92451	217.263	1026.098	296.466187	−14.814114	0.2258499	19.842	18.116	17.5660	17.281	M	dM0	5
92922	281.008	1772.730	296.510345	−14.817943	0.2701451	20.554	18.051	17.4380	17.145	M	dM3	5
93248	326.066	1540.433	296.496643	−14.820441	0.2566175	19.105	17.409	16.7510	16.619	M	dM0	6
93654	382.729	1723.071	296.507416	−14.823716	0.2675961	20.611	18.123	17.4570	17.226	M	dM3	5
95374	622.894	2208.565	296.536194	−14.837629	0.2975757	19.641	17.766	17.0430	16.905	M	dM1.5	5
96738	816.496	1589.804	296.499664	−14.848536	0.2629713	20.902	17.987	17.5020	17.164	M	dM4.5 e	5
97207	885.612	959.956	296.462311	−14.852363	0.2270565	19.562	17.407	16.6350	16.259	M	C5.5	5
97491	926.302	945.729	296.461395	−14.854693	0.2266777	20.143	17.256	16.2080	15.532	C	C6.5	6
98325	1048.711	844.282	296.455383	−14.861692	0.2225546	19.508	17.308	16.4480	16.242	M	M2III	5
98962	1135.729	2082.118	296.528748	−14.866978	0.2950821	20.061	18.105	17.3400	17.134	M	M1III	5
99857	1274.426	1372.990	296.486786	−14.874781	0.2563269	19.887	18.073	17.4180	17.156	M	dM1.5	5
100796	1419.893	1243.871	296.479126	−14.883121	0.2514958	19.599	17.210	16.4010	16.127	M	C5.5	5
101126	1471.182	1100.224	296.470612	−14.886045	0.2444083	20.072	17.665	16.7430	16.467	C	M3III	6
101466	1524.584	1278.832	296.481201	−14.888750	0.2552905	23.437	16.817	16.3000	15.970	M	dM4 5	
101959	1587.652	2163.375	296.533600	−14.892983	0.3063897	20.140	17.884	17.0380	16.830	M	M1III	5
102209	1630.584	509.353	296.436218	−14.895130	0.2160539	20.776	17.176	16.2120	15.618	C	–	4
102560	1682.059	1178.212	296.475250	−14.898197	0.2530735	19.993	17.130	16.1530	15.481	C	C5.5	5
102893	1730.912	1780.032	296.510925	−14.901115	0.287443	20.503	17.675	17.0830	16.767	M	dM3.5	6
104199	1937.366	2093.055	296.529480	−14.912703	0.3088658	21.613	17.331	16.7000	16.463	M	dM1.5	5
90330	39.236	341.283	296.251434	−14.798083	0.01209043	20.545	17.625	16.6160	16.058	C	C5.5	5
90637	80.620	516.378	296.261719	−14.800416	0.02134283	21.369	17.985	17.1260	16.916	M	M4III	5
90931	122.347	1115.506	296.297028	−14.802626	0.05644372	20.820	16.821	15.7580	14.954	C	C6.5	6
91224	161.925	878.662	296.283051	−14.804906	0.04248666	19.731	17.327	16.5590	16.317	M	S0III	4
91556	203.002	423.942	296.256256	−14.807403	0.01616204	20.364	17.424	16.3270	15.554	C	C6.5	6
91964	254.498	224.882	296.244385	−14.810474	0.008001597	21.079	16.872	15.9600	15.476	C	C5.5	5
92305	301.875	218.360	296.244141	−14.813117	0.01031772	20.921	17.320	16.1870	15.349	C	C8.2	5
92600	342.115	480.734	296.259552	−14.815343	0.02239389	20.168	17.428	16.3350	15.717	C	C6.5	5
92860	381.051	390.904	296.254303	−14.817538	0.01967468	20.773	18.297	17.3770	16.608	C	S0III	4
93164	421.773	634.683	296.268646	−14.819822	0.03249384	20.124	17.718	16.9390	16.700	M	M2III	5
93460	461.834	483.581	296.259796	−14.822150	0.02682021	19.839	17.409	16.4700	16.006	C	C5.5	5

ID	X [px]	Y [px]	RA [deg]	DEC [deg]	r [deg]	R [mag]	J [mag]	H [mag]	K [mag]	Sp. Cl. photometry	Sp. Cl. spectroscopy	Quality flag
93748	502.149	572.866	296.264984	−14.824442	0.03219609	20.889	18.374	17.3080	17.061	C	M0III	4
94448	601.895	579.621	296.265381	−14.830131	0.03643567	20.106	17.761	17.0260	16.760	M	M1III	5
94780	650.996	475.075	296.259155	−14.832942	0.03486604	19.663	17.482	16.7280	16.510	Mca	C5.5	6
95344	727.609	443.900	296.257324	−14.837327	0.03780291	20.378	18.011	17.1070	16.687	Cca	C5.5	6
95636	770.523	908.377	296.284698	−14.839629	0.0570606	20.585	17.812	16.9390	16.840	Mca	M1III	5
96024	821.577	454.113	296.257874	−14.842669	0.04287735	20.334	17.395	16.2650	15.595	Cca	C6.5	6
96296	861.206	230.208	296.244781	−14.845008	0.04178908	20.156	17.719	16.6780	16.005	C	C5.5	5
96667	910.498	529.546	296.262543	−14.847853	0.04955171	21.242	17.049	16.0520	15.442	Cca	C5.5	4
96968	963.377	1793.570	296.337067	−14.850516	0.1073543	19.090	16.924	16.0800	15.693	C	C5.5	6
97389	1018.552	752.407	296.275482	−14.853798	0.06127338	20.071	17.352	16.2710	15.605	C	C6.5	5
97697	1064.739	332.418	296.251160	−14.856455	0.05406864	20.846	17.765	16.9710	16.703	M	M	4
97991	1106.408	808.237	296.278717	−14.858888	0.06730009	19.844	16.683	15.6880	15.117	C	C5.5	6
98249	1146.769	511.304	296.261169	−14.861171	0.06129897	20.811	18.091	17.1980	16.647	C	C5.5	6
98545	1191.509	851.100	296.281311	−14.863727	0.07275971	20.309	18.471	17.4030	17.179	C	M0.5III	5
98847	1234.609	1396.118	296.313477	−14.866092	0.09612019	20.018	18.075	17.5980	17.160	M	–	4
99137	1278.045	1324.703	296.309265	−14.868592	0.09466992	19.455	17.326	16.5680	16.129	C	C5.5	6
99721	1366.676	1717.017	296.332581	−14.873631	0.1157177	19.819	18.135	17.3800	17.125	M	–	4
100035	1410.947	995.032	296.289734	−14.876258	0.08785845	20.120	17.404	16.5370	15.991	C	C5.5	5
100453	1477.075	783.396	296.277252	−14.880092	0.08497779	19.755	17.638	16.7340	16.552	M	M1III	5
100706	1517.643	529.845	296.262299	−14.882443	0.08194143	19.280	16.354	15.3960	14.905	C	C5.5	6
100979	1558.241	1069.597	296.294189	−14.884681	0.09733777	20.325	16.906	15.8260	15.156	C	C6.5	6
101729	1673.232	1356.833	296.311371	−14.891082	0.1126627	20.479	18.094	17.3270	17.085	M	–	4
102279	1753.532	217.862	296.244232	−14.895714	0.09235623	19.118	17.515	16.6780	16.557	M	–	4
102581	1795.498	545.039	296.263153	−14.898390	0.09760413	20.287	18.173	17.3070	17.075	M	C5.5	6
103184	1889.492	1652.989	296.328705	−14.903600	0.1334105	20.209	17.888	16.9520	16.837	M	M2III	5
103500	1941.249	339.905	296.251007	−14.906404	0.1034999	21.548	17.965	17.0860	16.770	C	C5.5	5
103941	2018.966	603.149	296.266968	−14.910404	0.1101786	21.533	17.840	16.5790	15.701	C	C8.2	5
107639	90.320	1848.383	296.340912	−14.947414	0.1754879	19.853	17.775	16.9080	16.764	M	M1III	5
107895	141.717	1260.647	296.306091	−14.950318	0.1608309	19.690	17.745	16.9440	16.937	M	M1III	5
108813	310.333	1929.862	296.345795	−14.960103	0.1887184	19.234	16.906	16.0730	15.723	C	C5.5	5
109046	356.210	938.537	296.286987	−14.962574	0.1657698	20.207	17.446	16.2970	15.629	C	C6.5	6
109316	408.847	976.886	296.289246	−14.965583	0.169296	18.844	17.313	16.7130	16.450	M	C	4
109686	475.700	1311.411	296.309082	−14.969496	0.1796363	20.771	18.226	17.7680	17.287	M	dM3.5	5
110010	537.418	1344.334	296.311035	−14.973057	0.1836735	20.228	17.364	16.3490	15.704	C	C6.5	5
111073	738.693	2153.645	296.359039	−14.984733	0.2165666	19.334	17.425	16.7540	16.575	M	dM1.5	6
111423	811.518	842.212	296.281311	−14.988668	0.1896614	19.220	17.160	16.3460	16.070	M	C5.5	6
111671	852.931	1568.073	296.324280	−14.991217	0.2055921	20.466	18.020	17.4530	17.201	M	dM3	6
111889	895.499	1744.780	296.334747	−14.993670	0.2122662	21.401	17.319	16.2390	15.529	C	C6.5	6
112261	964.857	1587.678	296.325409	−14.997616	0.2119024	19.962	17.490	16.6140	16.124	C	C5.5	5
112435	1004.553	928.719	296.286377	−14.999730	0.2015696	19.476	17.827	17.2740	17.038	M	dM0	5
112686	1047.426	1223.988	296.303833	−15.002280	0.2086652	19.381	17.512	16.7450	16.488	M	M0III	4
112903	1089.071	1245.400	296.305145	−15.004685	0.2113553	20.028	18.013	17.6660	17.264	M	dM1.5	5
113115	1129.684	1470.147	296.318451	−15.007016	0.2179673	21.764	18.252	17.6110	17.427	M	M5III	5
113364	1176.565	484.953	296.260254	−15.009410	0.2069169	20.194	17.864	17.2920	17.027	M	dM3	5
113623	1216.924	2051.431	296.352936	−15.012109	0.2369994	20.737	18.009	17.5350	17.204	M	dM3.5	5
113878	1277.141	315.562	296.250244	−15.015092	0.2118824	22.244	18.436	17.1400	15.842	C	C8.2	5
114236	1337.366	1651.943	296.329254	−15.018955	0.2330504	19.013	17.125	16.4880	16.326	M	dM1.5	6
114897	1466.873	1761.934	296.335785	−15.026363	0.2424075	18.650	17.007	16.3370	16.189	M	dM1.5	6
115382	1572.098	840.643	296.281281	−15.032146	0.2323079	20.944	17.265	16.7060	16.274	M	dM4.5	5
115893	1669.983	764.803	296.276825	−15.037701	0.2370571	20.411	18.149	17.5180	17.245	M	dM3	5
116640	1803.690	1112.014	296.297333	−15.045440	0.2485735	21.073	17.954	17.3490	17.134	M	dM4	5
117022	1885.855	409.945	296.255890	−15.049867	0.2469119	19.396	18.195	17.6640	17.390	M	dK7	5
117340	1960.154	464.028	296.259125	−15.054071	0.2513258	21.035	18.170	17.5590	17.261	M	dM	5
117545	2000.870	410.857	296.255951	−15.056370	0.2534064	20.322	17.074	16.4960	16.190	M	dM4.5	6
108786	347.254	1890.298	296.208069	−14.959845	0.1597604	20.334	18.136	17.2380	17.009	M	M	4
111185	807.063	2269.672	296.230438	−14.986133	0.1829852	20.142	18.298	17.5770	17.414	M	M	4
111623	884.891	2039.637	296.216919	−14.990644	0.1887049	20.257	17.631	16.6910	16.218	C	C5.5	6
112118	975.975	1659.463	296.194397	−14.995967	0.1980011	19.780	17.771	17.1630	16.854	M	dM3	5
112577	1068.983	2044.750	296.217194	−15.001184	0.1991336	20.855	18.346	17.5780	17.201	M	dM4.5	5
113378	1213.427	1690.476	296.196259	−15.009543	0.2108269	21.177	18.098	17.5000	17.103	M	dM	4
113721	1281.860	1956.581	296.211914	−15.013387	0.2119066	18.965	16.706	16.1730	15.871	M	dM3	6
90920	24.122	2067.737	296.219086	−14.802538	0.02152248	20.155	17.309	16.4770	15.994	C	C5.5	5
92178	187.130	2153.053	296.224152	−14.812045	0.0185589	21.067	17.551	16.6890	16.480	M	M4III	4
94985	584.671	2005.535	296.215454	−14.834577	0.04002473	19.666	17.326	16.5080	16.257	M	S	4
95289	629.275	1203.105	296.168030	−14.836925	0.07991805	21.080	18.081	16.8620	15.934	C	C6.5	6
95602	668.712	2110.321	296.221710	−14.839417	0.04063923	20.663	17.929	17.0000	16.501	C	C5.5	5
96812	839.958	1822.203	296.204712	−14.849141	0.05810992	20.326	17.306	16.2620	15.565	C	C6.5	6
97422	925.995	1528.273	296.187256	−14.854028	0.07351676	20.617	18.166	17.2240	16.937	C	C5.5	6
97682	964.318	1829.236	296.205139	−14.856238	0.06360424	19.475	17.242	16.4690	16.279	M	M0III	5
97984	1009.971	1505.292	296.185944	−14.858833	0.07781852	20.109	17.790	16.9170	16.746	M	M2III	5
99216	1188.823	2144.970	296.223785	−14.869195	0.06787854	19.977	17.820	17.0720	16.915	M	M0.5III	5
100106	1321.549	2200.657	296.227081	−14.876891	0.07469317	20.122	17.543	16.4570	15.858	C	C5.5	5
100585	1404.960	2198.103	296.226807	−14.881382	0.07916152	21.294	17.365	16.3690	15.908	C	C	4
101946	1609.342	1596.227	296.191498	−14.892875	0.1020319	21.547	17.543	16.6580	16.433	M	S	5
90134	27.600	907.319	295.976105	−14.796489	0.264576	20.471	18.250	17.4110	17.052	C	M1III	5
90520	84.943	2055.376	296.043884	−14.799508	0.1967451	20.468	17.434	16.7460	16.545	M	dM3.5	5
90866	126.883	674.756	295.962311	−14.802186	0.2782818	21.050	17.690	17.1830	16.897	M	dM3.5	5
91427	199.412	648.279	295.960724	−14.806342	0.2798811	22.188	17.602	17.0190	16.665	M	dM6 e	6
92657	361.760	1916.436	296.035767	−14.815892	0.2052018	22.154	17.822	16.8950	16.774	M	M1III	5
93057	423.404	690.692	295.963165	−14.819047	0.2778642	20.283	17.948	17.2510	17.002	M	dM2	5
94035	558.781	939.240	295.977814	−14.826708	0.2638051	19.779	17.060	16.4660	16.200	M	dM3	5
94682	656.412	1757.368	296.026215	−14.832167	0.2162926	19.749	17.658	16.9900	16.899	M	dM1.5	5
95365	750.591	1809.839	296.029327	−14.837542	0.2139993	20.596	18.035	17.4230	17.198	M	dM3.5	4
95693	792.880	1220.060	295.994385	−14.840031	0.2489108	19.860	18.069	17.3560	17.191	M	–	4
96052	835.129	876.072	295.974335	−14.842854	0.269158	22.364	17.510	16.8390	16.574	M	dM	4
96411	889.052	1484.176	296.010468	−14.845939	0.2340153	21.302	18.142	17.6840	17.415	M	dM	4

ID	X [px]	Y [px]	RA [deg]	DEC [deg]	r [deg]	R [mag]	J [mag]	H [mag]	K [mag]	Sp. Cl. photometry	Sp. Cl. spectroscopy	Quality flag
97334	1025.112	1006.412	295.981750	−14.853352	0.2636103	19.852	17.882	17.0400	16.800	M	M0III	5
97603	1067.237	1661.327	296.020447	−14.855683	0.2262595	20.116	18.329	17.3540	17.394	M	M0III	5
97963	1121.133	1734.382	296.024811	−14.858717	0.2227494	21.788	17.193	16.6130	16.227	M	dM6 e	6
98915	1261.224	2181.420	296.051331	−14.866667	0.1995443	20.285	17.404	16.4560	15.876	C	C5.5	5
99484	1347.357	342.303	295.942688	−14.871535	0.3055879	22.236	17.194	16.3980	16.158	M	M3III	5
100070	1432.050	1714.298	296.023621	−14.876556	0.2289607	19.508	17.214	16.6580	16.330	M	dM2	5
100499	1502.209	1325.995	296.000641	−14.880625	0.2520608	20.357	17.727	17.2400	16.872	M	dM3.5	4
100778	1544.422	2143.325	296.049103	−14.882938	0.2073375	20.125	18.103	17.2830	17.111	M	M0III	5
101968	1720.595	2017.875	296.041718	−14.893066	0.2181393	21.246	17.482	16.8840	16.529	M	dM4	5
102751	1838.349	2126.908	296.048126	−14.899792	0.2152396	19.983	17.296	16.4810	15.876	C	C5.5	6
103070	1894.591	1799.041	296.028839	−14.902554	0.2338036	22.678	17.350	16.1640	15.263	C	C8.2	5
103381	1934.731	2059.621	296.044067	−14.905341	0.2213757	20.697	18.504	17.7500	17.381	M	C5.5	6
107815	121.827	1758.182	296.027344	−14.949381	0.2584099	21.766	18.017	17.4250	17.123	M	dM	4
110171	584.100	1367.470	296.003693	−14.974893	0.2924378	20.379	18.392	17.5600	17.210	C	C5.5	5
110632	667.727	2162.411	296.050873	−14.979843	0.2590641	20.933	17.588	16.8800	16.654	M	dM4.5	5
111079	755.347	1732.773	296.025360	−14.984833	0.2814803	21.150	18.051	17.6140	17.256	M	dM4.5	4
111590	852.096	1197.049	295.993561	−14.990264	0.3097264	19.735	17.874	16.7020	15.840	C	C6.5	5
112033	934.863	1604.944	296.017761	−14.995077	0.2939073	19.866	17.849	17.0500	16.936	M	M1III	5
113019	1120.439	2073.050	296.045563	−15.005780	0.281036	19.959	17.290	16.6870	16.406	M	dM3.5	6
113319	1178.112	1928.772	296.036987	−15.009061	0.289376	20.085	17.369	16.6480	16.493	M	dM3.5	6
113914	1293.872	955.777	295.979340	−15.015457	0.3364627	19.019	17.607	16.8720	16.668	M	dM0	6
114276	1361.872	1199.123	295.993744	−15.019435	0.3280111	19.883	17.743	17.0910	16.938	M	dM3	6
114879	1476.614	2254.131	296.056305	−15.026172	0.2890936	20.169	17.870	17.1500	17.096	M	dM2	5
115433	1590.278	2011.476	296.041931	−15.032643	0.3033219	20.700	17.826	17.1900	16.948	M	dM4.5	5
115804	1662.083	1643.314	296.020050	−15.036669	0.3209961	19.639	17.751	17.0080	16.689	M	C8.2	5
115993	1702.926	1214.034	295.994659	−15.038876	0.340466	19.993	18.321	17.6930	17.438	M	dM1.5	5
116596	1808.469	1669.099	296.021637	−15.045016	0.3260435	19.021	17.040	16.2820	16.056	M	C5.5	5
116999	1891.919	955.323	295.979401	−15.049569	0.3588932	20.682	17.948	17.2260	17.089	M	dM4.5	4
117181	1932.168	1987.050	296.040497	−15.052125	0.3191968	19.601	17.159	16.4980	16.321	M	dM3	5
117434	1984.157	1982.665	296.040161	−15.055114	0.3217403	20.201	18.430	17.3620	17.348	M	M	4
55322	299.439	284.508	297.102814	−14.442153	0.9348535	25.650	18.075	17.5120	17.107	M	–	4
55631	381.046	1621.253	297.181274	−14.445981	1.006308	19.449	18.530	18.2640	17.292	C	–	3
56243	516.498	2213.528	297.216156	−14.453639	1.036379	19.871	17.765	17.0210	16.866	M	dM1.5	5
58261	991.769	1182.882	297.155334	−14.481108	0.96987	18.856	18.038	17.2590	17.179	M	–	3
59120	1205.369	367.935	297.108337	−14.493650	0.9213839	17.725	18.191	17.3830	16.661	C	–	3
59314	1257.450	1245.088	297.158966	−14.496314	0.9683669	20.093	17.297	16.7560	16.449	M	dM3	5
59700	1331.910	2207.370	297.215637	−14.500302	1.021079	21.480	18.073	17.5880	17.286	M	dM4	4
60058	1393.095	1587.712	297.179169	−14.503994	0.9851864	19.245	17.677	16.9810	16.811	M	dM1.5	5
61046	1554.100	1102.296	297.150513	−14.513336	0.9550467	21.495	17.780	17.2830	16.918	M	dM6 e	6
41793	128.679	1273.751	297.161224	−14.292459	1.052928	19.643	17.802	17.0750	17.045	M	dM1.5	5
42043	167.830	1827.443	297.193909	−14.294868	1.080487	19.562	17.032	16.4650	16.212	M	dM3	6
42791	304.420	1257.767	297.160309	−14.302498	1.04729	19.652	18.161	17.4660	17.205	M	dM0	5
43020	344.109	1481.087	297.173523	−14.304831	1.057811	20.250	17.817	17.3300	17.050	M	dM2	5
43232	384.173	1826.030	297.193878	−14.307225	1.074699	19.726	17.774	17.1210	16.909	M	dM1.5	5
43515	433.154	2111.488	297.210724	−14.310122	1.088353	20.046	17.649	17.0180	16.718	M	dM3	6
44628	632.366	1484.693	297.173767	−14.321322	1.050356	21.117	18.275	17.7930	17.289	M	dM5 e	4
44997	696.509	2007.250	297.204651	−14.325150	1.076181	18.761	17.781	17.1250	17.029	M	dK7	5
45410	773.367	1441.205	297.171265	−14.329375	1.044454	20.780	17.739	17.0680	16.905	M	dM4.5 e	6
45954	878.200	1071.252	297.149353	−14.335320	1.022241	17.687	17.041	16.7730	15.965	M	K	4
46279	936.157	2125.464	297.211639	−14.338922	1.076431	20.688	18.101	17.4830	17.153	M	dM4.53	5
46592	1002.633	1272.386	297.161255	−14.342500	1.029602	18.900	16.410	15.7430	15.544	M	dM3	6
47107	1091.427	2031.820	297.206085	−14.347786	1.06761	20.596	17.681	17.0740	16.879	M	dM3	5
47505	1173.800	903.516	297.139404	−14.352262	1.005693	20.581	18.128	17.6650	17.304	M	dM3	5
48194	1308.802	1149.205	297.153961	−14.360078	1.015287	21.736	17.469	16.9170	16.496	M	dM6 e	6
49612	1594.097	2114.281	297.211029	−14.376673	1.060129	21.670	17.190	16.6100	16.226	M	dM6 e	6
49967	1656.005	1965.697	297.202271	−14.380200	1.050692	20.526	18.048	17.3940	17.222	M	dM3	5
40802	59.545	618.549	296.948669	−14.282547	0.8790305	19.164	17.247	16.6170	16.438	M	dM1.5	5
41060	105.735	678.351	296.952179	−14.285142	0.88033	18.795	17.218	16.6020	16.371	M	dM0	5
41596	206.230	1344.224	296.991333	−14.290698	0.9091253	20.862	17.848	17.3140	16.943	M	dM3.5	5
42248	316.713	1814.475	297.019135	−14.296878	0.9288309	21.572	18.136	17.5200	17.298	M	dM3.5	4
42535	366.448	892.736	296.964722	−14.299945	0.8819659	19.808	16.726	16.2040	15.882	M	dM3	5
42901	427.853	194.631	296.923645	−14.303656	0.8463674	19.951	17.635	17.0440	16.813	M	dM1.5	5
43108	467.457	409.896	296.936279	−14.305859	0.8553126	19.490	17.659	17.0290	16.808	M	dM1.5	5
43348	512.920	305.263	296.930145	−14.308464	0.8488092	20.577	17.777	17.4400	16.951	M	dM3	5
43605	562.136	1913.757	297.024963	−14.310925	0.9261759	19.963	17.856	17.2600	16.923	M	dM1.5	5
43915	614.424	992.529	296.970581	−14.314083	0.8788327	20.087	18.075	17.4360	17.237	M	dM1.5	5
44174	664.135	448.409	296.938538	−14.317039	0.8507099	20.701	17.720	17.0690	16.846	M	dM3.5	5
45366	876.289	1954.226	297.027313	−14.328870	0.9187708	21.988	18.067	17.6230	17.274	M	dM	4
45624	924.062	776.802	296.957794	−14.331817	0.8583705	20.741	17.547	17.1000	16.708	M	dM3.5	5
45931	984.121	1414.710	296.995422	−14.335114	0.8883079	20.621	17.862	17.3230	17.010	M	dM3.5	5
46352	1063.054	1053.418	296.974060	−14.339691	0.867774	21.622	18.259	17.7840	17.415	M	dM	5
46864	1165.936	1695.130	297.011963	−14.345500	0.8970596	19.885	18.038	17.3540	16.989	M	dM0	5
47209	1223.670	1728.200	297.013916	−14.348797	0.897064	20.879	18.201	17.5520	16.944	C	–	4
47435	1264.705	1426.591	296.996124	−14.351164	0.8805543	20.997	18.032	17.5270	17.282	M	dM3	4
48481	1483.091	773.294	296.957520	−14.363795	0.8409918	22.152	18.022	17.2810	17.010	M	dM	5
48886	1570.574	896.634	296.964783	−14.368781	0.8446152	19.889	17.611	17.0000	16.747	M	dM1.5	5
49384	1657.565	521.578	296.942719	−14.373831	0.8231282	21.102	17.839	17.1140	16.891	M	dM4	5
49732	1727.162	318.647	296.930756	−14.377884	0.8108132	21.521	17.241	16.7240	16.363	M	dM4.5 e	6
50075	1792.846	447.832	296.938354	−14.381606	0.8153586	20.596	17.528	16.9020	16.637	M	dM3	5
50524	1888.690	1181.466	296.981598	−14.386964	0.8500214	21.985	18.128	17.5470	17.365	M	dM	5
51221	2027.914	1598.493	297.006256	−14.394895	0.8678392	20.348	18.126	17.2970	17.202	M	dM3	5
54857	195.586	1906.440	297.025116	−14.436872	0.8659362	20.694	17.775	17.1920	16.831	M	dM3	6
55755	369.242	1049.854	296.974823	−14.447328	0.8160309	22.166	17.896	17.2830	17.053	M	dM	4
56605	567.635	1957.577	297.028107	−14.458230	0.8598522	19.843	17.570	17.0790	16.704	M	dM1.5	6
57180	697.686	1060.390	296.975769	−14.466044	0.8088987	18.471	18.236	17.5140	17.185	M	–	4
57342	739.583	1797.938	297.018646	−14.468082	0.847248	19.104	16.712	16.0680	15.835	M	dM2	5

ID	X [px]	Y [px]	RA [deg]	DEC [deg]	r [deg]	R [mag]	J [mag]	H [mag]	K [mag]	Sp. Cl. photometry	Sp. Cl. spectroscopy	Quality flag
57732	827.898	708.120	296.954742	−14.473660	0.7866137	22.591	18.343	17.8040	17.385	M	K	3
57978	896.278	1725.470	297.014343	−14.477056	0.8397698	21.46	18.167	17.5550	17.215	M	dM	4
58422	1006.956	957.693	296.968933	−14.483230	0.7956201	20.872	17.727	17.0760	16.816	M	dM	4
59131	1188.569	1876.573	297.023346	−14.493817	0.8417642	21.156	18.165	17.5550	17.168	M	dM	4
60052	1366.221	1754.735	297.016083	−14.503956	0.8313085	21.259	18.178	17.6320	17.433	M	dM	4
60786	1487.377	1799.477	297.018768	−14.510902	0.8313443	20.503	18.148	17.6510	17.346	M	dM3	5
61414	1597.897	427.123	296.937805	−14.516788	0.7538383	19.436	17.791	17.1000	16.940	M	dM0	5
61782	1657.570	1600.655	297.006958	−14.520561	0.8169055	20.277	17.413	16.7880	16.564	M	dM3	5
62104	1705.797	1828.993	297.020477	−14.523369	0.8286481	20.379	18.044	17.3630	17.141	M	dM3	5
62393	1762.292	696.747	296.953674	−14.526256	0.7650582	20.050	18.052	17.4470	17.269	M	dM1.5	5
62691	1812.163	336.567	296.932526	−14.528950	0.7443886	18.610	16.632	15.9790	15.793	M	dM1.5	6
63105	1876.585	1788.570	297.018127	−14.533105	0.8231884	18.940	17.651	17.0460	16.895	M	dK7	5
63424	1938.155	1067.854	296.975586	−14.536401	0.7819996	20.393	17.165	16.6410	16.351	M	dM4.5	5
63663	1980.842	887.455	296.964935	−14.538761	0.7711843	18.523	16.722	16.0230	15.882	M	dM1.5	6
136956	256.335	1523.124	295.645844	−15.270988	0.7565274	21.027	18.097	17.5640	17.253	M	dM3.5	4
139836	857.547	1398.050	295.638458	−15.305284	0.78385	18.308	17.652	16.9110	16.703	M	dK	4
142268	1410.831	973.393	295.612732	−15.336275	0.8234864	18.072	17.830	17.1280	16.957	M	dK	4
142730	1509.938	1521.907	295.644928	−15.342483	0.8033628	17.846	17.427	16.7960	16.615	M	dK	4
143023	1590.810	614.538	295.591583	−15.346883	0.8464938	18.352	16.991	16.2760	15.991	M	dK	4
143950	1808.174	1065.145	295.618652	−15.359362	0.8341869	21.326	17.498	16.8920	16.726	M	dK	4
144255	1871.771	479.626	295.584229	−15.363297	0.8627058	18.206	17.197	16.5530	16.344	M	dK	4
128247	1040.452	1126.373	295.622314	−15.175920	0.7218132	20.969	18.314	17.5150	17.276	M	M	4
129250	1218.280	2169.862	295.683594	−15.186219	0.6758493	21.990	18.208	17.5960	17.426	M	dM	4
126166	668.011	2267.463	295.689667	−15.155052	0.6535705	24.553	17.736	16.7870	16.428	C	–	4
131608	1653.595	2241.736	295.688568	−15.211617	0.6865458	20.194	17.775	17.1530	16.833	M	dM0	4
123364	216.995	1359.148	295.460785	−15.123086	0.8427787	20.475	18.389	17.7120	17.401	M	dM	5
124511	445.084	1274.828	295.456573	−15.136149	0.8516953	18.275	17.643	16.9520	16.724	M	dM0	5
125420	625.915	1428.566	295.464996	−15.146566	0.8481089	19.330	17.472	16.7390	16.559	M	dM0	5
130615	1574.202	904.421	295.434204	−15.201089	0.8991058	19.391	16.736	16.0630	15.827	M	–	4
131365	1726.452	2073.666	295.503571	−15.209061	0.8412692	18.599	18.138	17.3880	17.182	M	dM0	5
137212	288.103	1754.533	295.485199	−15.273877	0.889908	19.066	17.789	16.9970	16.800	M	K7III	4
139197	703.094	593.642	295.416962	−15.297790	0.9606015	21.676	18.304	17.5610	17.378	M	dM	4